



Suspension and Solution Precursor Plasma and HVOF Spray: A Review

Garima Mittal¹ · Shiladitya Paul^{1,2}

Submitted: 17 September 2021 / in revised form: 23 December 2021 / Accepted: 19 January 2022 / Published online: 11 March 2022
© The Author(s) 2022

Abstract Thermal spray, being a cost- and time-efficient process, is used extensively in industrial and engineering sections for mass production of desired coating structures, allowing to deposit a wide range of materials on various substrates. Conventionally, powder feedstocks are used in plasma and high-velocity oxy-fuel (HVOF) thermal spray that has limitations such as limited feedstock particle size (10–100 μm), clogging and limited options for coating materials. Liquid feedstocks, in the form of suspensions or precursor solutions could potentially resolve these issues by allowing nano- and submicron particles to be deposited, where unlike dry feedstock, the liquid medium helps in reducing the friction and avoiding the clogging. Also, liquid feedstocks, especially precursor solutions, provide the opportunity to deposit a wide range of coating materials with better control over coating microstructure, material composition and stoichiometry by varying the properties of the feedstock. Despite benefits, liquid feedstock has its own complexities, such as complex feedstock preparation, thermo-physical reactions during interaction with the energy source and gases. Therefore, it becomes essential to understand how different suspension and solution precursor feedstock properties affect the coating microstructures and properties. This review paper covers a detailed discussion on the role of different process parameters such as

feedstock properties, injection methods, different torches and surface properties, affecting the coating quality and performance and related recent developments and challenges are discussed. This would be beneficial in optimizing the spray parameters to obtain coatings with desired microstructures. The later part of the review focuses on the economic aspect of the suspension/solution precursor-based plasma and HVOF spray methods and their various applications.

Keywords liquid feedstock properties · process parameters · solution precursor plasma spray · solution precursor HVOF spray · suspension plasma spray · suspension HVOF (S-HVOF) spray

Abbreviations

St	Stokes number
We	Weber number
ρ_p	Specific mass of the particle
d_p	Diameter of the particle
v_p	Velocity of the particle
μ_g	Molecular viscosity of the gas
Re	Reynolds number
RGS	Ratio of the gas flow rate and suspension feed rate
F_D	Drag force
F_A	Adhesion force
ρ_l	Specific mass of the liquid droplet
v_l	Velocity of the liquid droplet

Introduction

The thermal spray process has evolved with time, and based on the thermal energy source, it can be divided into plasma spray, flame/combustion spray and electric arc

✉ Garima Mittal
gm323@leicester.ac.uk

✉ Shiladitya Paul
shiladitya.paul@twi.co.uk

¹ Materials Innovation Centre, School of Engineering, University of Leicester, Leicester, UK

² Materials and Structural Integrity Technology Group, TWI, Cambridge, UK

spray, where powder and wires are used as conventional feedstock. This review focuses on plasma spray and high-velocity oxy fuel (HVOF) spray.

In plasma spray, a plasma plume is used as a high-enthalpy source, while in HVOF, thermal energy is generated from fuel combustion in the presence of oxygen. Thermal energy in plasma spray is higher than the HVOF spray, which helps in the sufficient melting of feedstock powder. While the kinetic energy of feedstock powder is higher in HVOF spray than plasma spray due to the supersonic speed of the flame, and hence, the formed splats are comparatively thinner, and formed coatings are comparatively denser and well-adhered than in plasma spray. Based on the coating requirements, plasma source gas can be changed i.e., argon, a mixture of argon and hydrogen, or argon, hydrogen, and nitrogen. For HVOF, different fuels can be used, such as kerosene, hydrogen, ethylene or propylene. Most of the HVOF guns support axial (parallel to the gas flow) injection of the feedstock that allows particles to be in contact with the heat source for a longer time. A better exchange of kinetic and thermal energies in axial injection increases the deposition efficiency (Ref 1). Feedstock injected radially (perpendicular to the gas flow) into the plasma plume or flame, due to being in contact with the heat source for a shorter period, experience insufficient melting and speed.

Despite the commercial availability of powder feedstocks in various sizes, the powder spray technology is limited to 10–100 μm size powder due to poor flowability and nozzle clogging. Particles smaller than 10 μm due to having a low moment of inertia do not follow the trajectories of the gas streamlines that makes it difficult to insert them into the high-enthalpy zone (core) (Ref 2). Consequently, these particles pass the substrate without hitting and depositing on it. Particles with smaller sizes more frequently clog the injection nozzle due to their high fraction and low flowability. Besides, additional efforts are required to segregate (sieve) the particles with a particular size. These shortcomings affect the quality of the coating by introducing micro-defects in the form of unmelted particles, poor adhesion between stacks of splats and pores (Fig. 1) (Ref 3).

The liquid feedstock-based plasma/HVOF spray could resolve these issues, offering various advantages such as allowing to deposit a wide range of coating materials, providing a better control of coating microstructures and depositing coatings with specific microstructures and desired properties (Ref 4).

Suspension Plasma/HVOF Spray

In a suspension plasma/HVOF spray, instead of a dry powder, particles suspended in a liquid medium are used as

a feedstock. Commonly used suspension media are water, ethanol, propanol, or a mixture of these. The use of liquid medium allows to spray particles even with a smaller size ($<10 \mu\text{m}$) and resolve the nozzle clogging issue by exhibiting better flowability than the dry powder (Ref 3). However, there are other factors such as solid content in the suspension medium that influence the clogging. Once suspension droplets are fed into the system, after coming into contact with plasma plume or flame, fragmentation of droplets takes place. Later, the solvent vaporizes and agglomerates of coating material due to the high-enthalpy sinter and melt. Due to the acceleration toward the substrate, these feedstock droplets hit the substrate and form splats, and continuous stacking of splats develop coating. Depending on the suspended particle size and shape, the flow rate of feedstock and the nature of the suspension medium, interactions between suspension and heat source also vary along with the coating properties (Ref 5, 6).

Solution Precursor Plasma/HVOF Spray

A liquid feedstock could also be in the form of a precursor solution of the desired coating materials. In solution precursor thermal spray, when the solution precursor feedstock droplets are introduced into the system, the evaporation of the solvent, followed by precipitation of precursors due to the high enthalpy of plasma/flame takes place. After melting, these precipitates travel toward the substrate. The Solution precursor plasma/HVOF spray provides several benefits over the suspension plasma/HVOF spray, such as resolving the particle agglomeration and sedimentation issues and better control over the coating morphology and chemistry by altering the chemical composition, concentration, and stoichiometry of the precursor solution (Ref 7). However, the deposition efficiency of solution precursor thermal spray is lower than the suspension plasma/HVOF spray. Also, to date, only the oxides have been possible to deposit using solution precursor processes.

The suspension and solution precursor plasma spray techniques are often called SPS and SPPS, respectively, and suspension and solution precursor HVOF spray techniques are S-HVOF. These liquid feedstock-based plasma and HVOF techniques are continuously drawing attention due to the versatility to choose the particle size, stoichiometry and chemical composition of the liquid medium. The coating morphology and properties depend on several parameters involved in spraying, such as preparation and insertion of the suspension or solution precursor, suspension medium or solvent and its viscosity, the interaction of liquid feedstock with the energy source, etc. Compared to the conventional powder-based thermal spray, the obtained thin coatings are denser with finer grains, show better splat

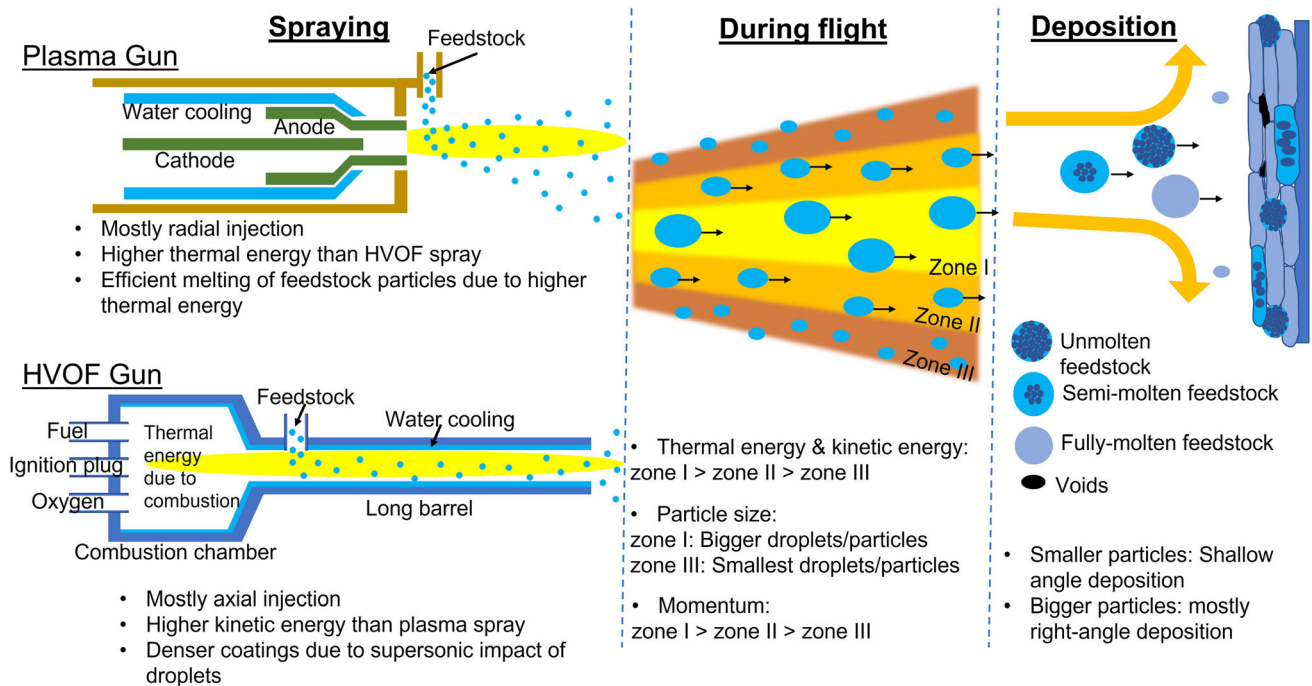


Fig. 1 Schematic representation of powder-based plasma and HVOF spray processes

adhesion and unique morphology because of the complex thermochemical and thermophysical changes occurring during spray.

An illustration depicting different thermochemical processes occurring in suspension-based and solution precursor-based thermal spray is presented in Fig. 2.

Physical and Chemical Processes During Spray

In powder and liquid feedstock-based thermal spray, the primary phenomenon is the same. However, the feedstock preparation, introduction of feedstock into the heat source and its interaction with plasma/flame is more complicated in suspension-/solution-based thermal spray, which affect the coating formation significantly. For instance, because of the low moment of inertia, suspended fine particles might get bounced back from the substrate and travel parallel to the substrate by following the gas trajectory, and consequently, give rise to the cauliflower-like features (Fig. 3) (Ref 9). The flow behavior of feedstock droplets in the gas stream is illustrated by Stokes number (*St*), defined as the ratio of the characteristic time of a particle (or droplet) to a characteristic time of the flow (equation):

$$St = \frac{\rho_p d_p^2 v_p}{18 \mu_g l}$$

where, ρ_p , d_p and v_p are the specific mass (kg/m^3), diameter (m) and velocity (m/s) of the particle. The μ_g is the molecular viscosity (Pa s) of the gas, and l (m) is the flow

boundary layer thickness from the substrate. The *St* value quantifies whether a particle would pursue the flow trajectory or not.

When $St \ll 1$, particles follow the fluid streamlines closely and pass parallelly to the substrate or hitting it at shallow angles. Contrarily, particles deviate from the gas flow path and deposit on the substrate if $St \gg 1$ (Fig. 3) (Ref 8). The suspension medium or solvent also influences the thermal and kinetic energies of feedstock droplets as besides melting, during flight, other phenomena such as the aerodynamic breakdown of liquid feedstock droplets, evaporation of liquid or heating and precipitation (in case of precursor feedstocks) and sintering also take place (Ref 10).

The aerodynamic breakup that takes place immediately after the injection of liquid feedstock, fragments larger droplets into smaller ones due to acceleration, drag force and shear deformation. The breakup geometry of the liquid stream depends upon two things: Reynolds number (the ratio between inertial forces and viscous forces; *Re*) and Weber number (the ratio between inertial forces and surface tension forces; *We*). After immediate evaporation of the suspension medium, rapid agglomeration/sintering of fine particles takes place. Let us assume that a particle travels at 500 m/s (velocity) for a 100 mm stand-off distance, and the diffusion coefficient of a material is $1.0 \times 10^{-10} \text{ m}^2/\text{s}$ at 1200 °C. Then, in 0.2 ms, the diffusion distance could be $\sim 140 \text{ nm}$. Consequently, a rapid

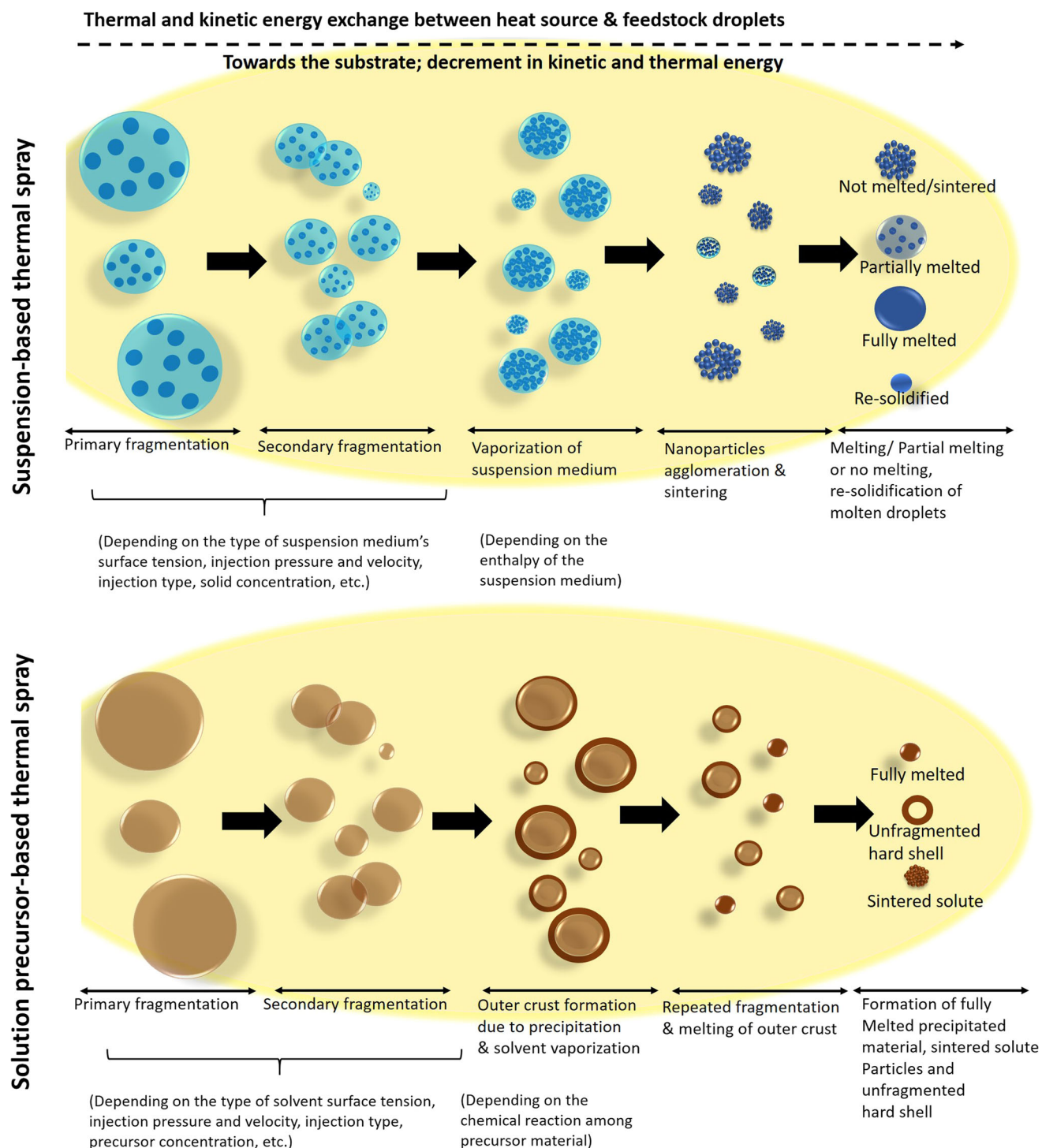


Fig. 2 An illustration of different thermochemical and thermophysical processes occurring in suspension-based and solution precursor-based thermal spray. Inspired by (Ref 8)

agglomeration of droplets due to the attraction forces at very short interparticle distance takes place.

In precursor solution feedstocks, droplets go through an additional and complex chemical change, during which the precipitation of solid particles occurs because of the

evaporation and super-saturation of the solvent. Later, melted droplets of these particles deposit on the substrate in molten or semi-molten form. Since finer particles exhibit rapid heating and cooling curves during their in-flight behavior, smaller standoff distances are preferred in SPS/

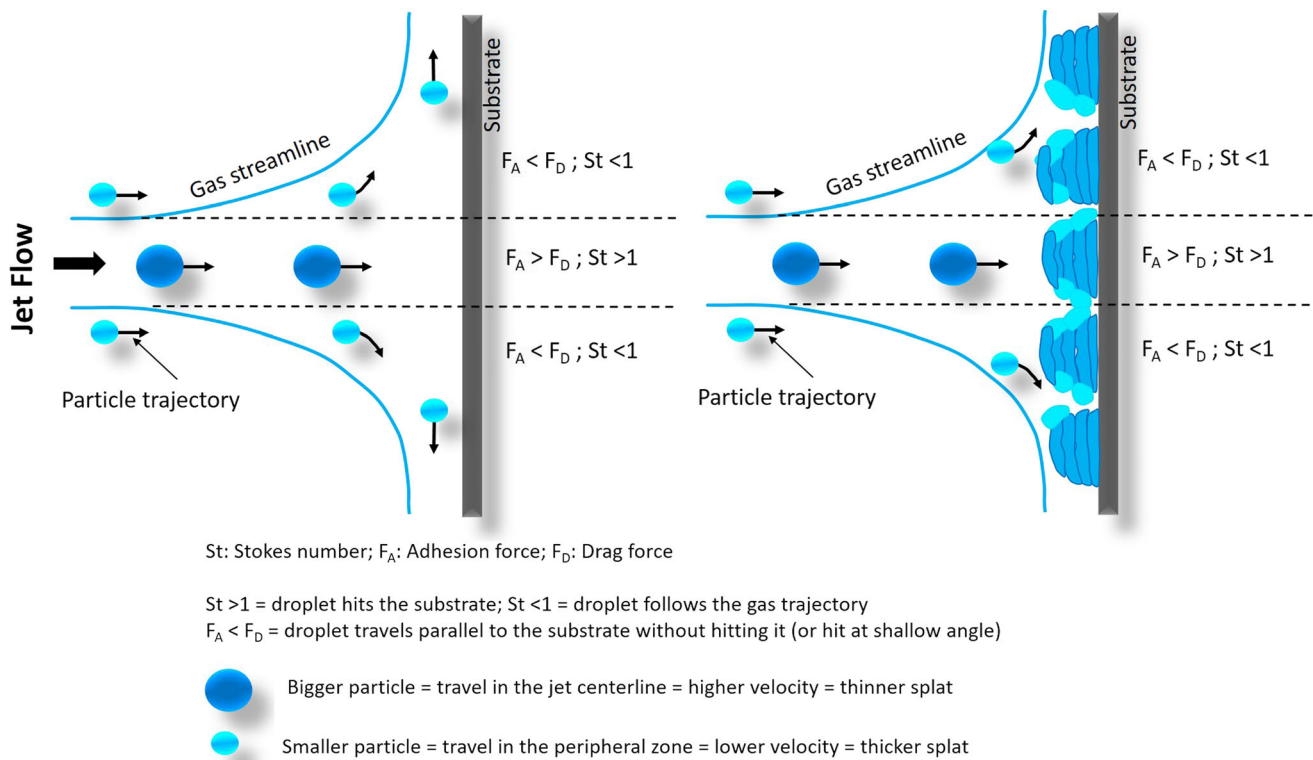


Fig. 3 Schematic representation of particle behavior in the presence of plasma/flame jet stream. Inspired by (Ref 11)

SPPS (50–120mm) and S-HVOF (100 to 200mm) (Ref 12). The time duration involved in evaporation and sintering is affected by the size of the droplet, suspension medium, viscosity of the medium and feedstock insertion conditions. Hence, liquid feedstock-based thermal spraying provides a high degree of freedom in developing desired and controlled coatings.

Feedstock

The first crucial step toward developing uniform and homogenous coating using liquid feedstocks is to understand the role of different parameters that affect feedstock preparation. Due to the lack of suitable diagnostic tools, detailed analysis of splat formation and the factors affecting its properties is a tedious task.

Liquid feedstocks can be divided into three categories, suspension, solution precursors, and hybrid feedstocks, and their properties (stability, viscosity, surface tension and chemistry) are affected by various factors that ultimately affect the coating morphology and properties. Particles for the suspension and suspension feedstocks can be purchased commercially or prepared in the laboratory (Ref 13, 14). The commercial feedstock could be in the form of powders (with or without dispersant) premixed in the solution or

powder along with dispersing agent ready to be mixed with the desired suspension medium.

Role of Particle Size and Shape in Suspension Feedstock

The size of particles suspended into the liquid medium is one of the critical factors that affect the degree of melting of particles and the coating density and efficiency (Ref 15). For suspension plasma spray and HVOF, a colloidal suspension is prepared by suspending fine particles (submicron to several nanometers in diameter) into an aqueous/alcoholic medium. Nanoscale particle forms a comparatively stable suspension than bigger particles, as latter has the tendency to sediment. However, nanomaterials have the tendency to form agglomerates in the suspension medium. Hence, these particles are further treated mechanically (mixing, sonication or ball milling) or chemically (using dispersant) to break agglomerates or reduce the particle size.

It is worth mentioning that the particle velocity and trajectory fluctuate with the particle diameter, and the size of the final particle is entirely different (usually smaller) and independent of the primary droplet. Primary droplets with $>10\mu\text{m}$ size are further broken into smaller droplets and the one with $<10\mu\text{m}$ size goes through intense

evaporation of suspension medium (Ref 3). During interaction with a high-enthalpy source, evaporation of the suspension medium takes place, and consequently, suspended particles come closer, followed by melting and agglomeration. Hence, the particle size near the substrate is different from the feedstock droplet. While following the gas track, smaller particles travel parallel to the substrate and deposit on its prominent asperities, giving rise to the porous columnar structure (also called the shadowing effect) (Ref 16). Larger particles following the gas trajectory (for $St \gg 1$), participate in coating formation by impacting the substrate at right angles. Therefore, coatings developed using a suspension feedstock with smaller particles exhibit prominent peak-valley features.

With the increased distance from the torch, the temperature decreases, and smaller particles re-solidify before hitting the substrate and form granular structures in the coating (Ref 17–19), while larger particles form larger splats with better wettability.

Many computational studies have been performed to understand the effect of particle size and shape in droplet formation (Ref 19–21). In one study, the in-flight behavior of spherical and non-spherical particles (usually obtained after high energy ball milling) during conventional HVOF spray was compared. It was found that non-spherical particles tend to follow the centerline trajectory of the gas flow and felt higher aerodynamic drag forces, which led to lesser dwell time during the flight than the spherical particles (Ref 20). The short period of contact with the heat source formed poorly melted droplets. Although this study was performed on powder feedstock, there could be a similar trend in suspension feedstocks.

It can be concluded that suspension feedstocks with large (submicron) particles form well-adhered coatings. While coatings with columnar and nanoscale porosity are formed with feedstock with fine (nanoscale) particles suspension. However, it is not as straightforward as it seems because coating properties and performance depend on various other parameters.

Role of Solid Content in the Suspension Feedstock

The solid content in a suspension feedstock affects the particle velocity and temperature and, ultimately, the coating microstructures (Ref 22, 23). Usually, higher solid content is preferred due to the deposition of thicker layer per pass i.e., higher material deposition rate. Similarly, using high solid content (or lower liquid medium) in feedstock could be cost- and energy-efficient as less energy is required to evaporate the suspension medium. (Ref 24–26). Sometimes, the coatings developed using a feedstock with higher solid content are thicker. This behavior could be explained as when more solid materials interact with

plasma/flame, less heat is distributed among the particles that form comparatively viscous droplets. When particles move away from the plasma or combustion torch, thermal and kinetic energies decrease so the decreased velocity does not provide enough momentum for the splat deformation. Hence, a less flattened splat is formed (Ref 24). However, there are other factors such as surface tension and viscosity that also influence the droplet fragmentation as well as splat formation.

The viscosity of the suspension feedstock also increases with the increased solid concentrations, complicating the atomization during the aerodynamic breakup. Hence, larger droplets containing the more significant mass concentration are formed, which follow the flow trajectory near the substrate and produce less columnar coatings by impacting the substrate perpendicularly (Ref 27).

Porosity also varies with particle content. Some of the examples of SPS and S-HVOF coatings with solid content in the feedstock and coating porosity are given in Table 1. In a recently reported study by Carnicer et al. (Ref 26), the increase in solid concentration (up to ~ 66 wt.%, which is higher than other studies), resulted in porous coatings (Ref 26). This was explained by insufficient melting of particles due to the increased particle concentration in the hot zone, leading to the generation of a smaller number of fully melted particles. Partially melted particles resulted in developing irregularities in the coating, such as voids or cracks.

In short, the higher concentration of particles in suspension feedstocks usually provides coatings with higher deposition efficiency but up to a limit. Beyond that, problems like increased viscosity of the suspension, agglomeration, sedimentation of particles, clogging of injector, inefficient melting of particles during flight occur and give rise to irregular coatings. Therefore, it is essential to optimize the suspension feedstock in terms of particle stability.

Role of Viscosity of Suspension Feedstock

The homogenous dispersion and stability of particles into the suspension are crucial for achieving uniform coatings. Because of the interparticle interactions, suspended nano and submicron particles tend to form agglomerates. To resolve the issue, dispersants are used that affect the viscosity of the suspension. The increased viscosity of the suspension obstructs the atomization and forms bigger droplets after secondary atomization. Bigger droplets, due to following the core trajectory of plasma/flame jet, obtain higher enthalpy and velocity (Ref 34). Suspensions with lower viscosity produce coatings with shadow effect due to the formation of smaller droplets that hit the substrate on shallow angles (Ref 35). While comparing the effect of viscosity and surface tension, Tarasi et al. (Ref 35) found

Table 1. Examples of suspension plasma spray and HVOF spray coatings comparing solid content in the suspension feedstock and porosity in developed coatings

Suspended material	Solid content (wt.%)	Average particle size (μm)	Spray method (R or A)*	Porosity	Reference
Al_2O_3	25	1.2	SPS (R) & S-HVOF (A)	#15 vol.% & 4 vol.%	(Ref 28)
	40	2.2	SPS (A)	6 vol.%	
Hydroxyapatite	23	4-5	SPS (A)	#6 area %	(Ref 29)
	13	0.3–0.6		21 area %	
8YSZ	25	0.1-1	SPS (A)	#516-45 area%	(Ref 30)
Cr_2O_3 + 0.2 wt% Graphene nanoplatelets	20	...	S-HVOF	&1.8 \pm 0.3 vol.%	(Ref 31)
$\text{Al}_2\text{O}_3/\text{TiO}_2$ coatings		0.8-1.8	S-HVOF (A)	#1 vol.%	(Ref 32)
$\text{Al}_2\text{O}_3/0\text{wt.}\% \text{TiO}_2$		0.6-1.7		3 vol.%	
$\text{Al}_2\text{O}_3/13\text{wt.}\% \text{TiO}_2$		0.5-1.0		1 vol. %	
$\text{Al}_2\text{O}_3/40\text{wt.}\% \text{TiO}_2$					
TiO_2	20	5.67	S-HVOF (R)	#<2 vol.%	(Ref 33)

*R and A stand for radial and axial spray.

Porosity measurement through: # = image analysis; \$ = Mercury infiltration porosimetry (MIP); & = not mentioned.

that the feedstock with lower viscosity formed more columnar coatings due to the smaller droplets formation after fragmentation that after deviation from the gas trajectory hit the substrate at shallow angle. Even though the viscosity affects the atomization process and the droplet formation, the coating microstructures are controlled by another significant suspension property, i.e., surface tension (see section 2.1.4.).

When the higher solid content is used, particle sedimentation becomes an issue (especially for coarse particles), hindering the potential use of a high concentration of material in the feedstock (Ref 27). Therefore, typical dispersants such as polyvinyl alcohol (PVA), polyacrylic acid (PAA), polyethylenimine (PEI), polyvinylpyrrolidone (PVP) and polyethylene glycol (PEG) are used that get adsorbed onto the particle surface, restricting the agglomerate reformation. Although, with time, the sedimentation trend increases, it can be resolved by shaking or stirring. Continuous stirring during the entire spray process could improve the coating quality. However, an excessive dispersant can also increase the suspension viscosity, and hence, it should be in optimal quantity.

Role of Dispersion Medium in Suspension Feedstock

The suspension medium affects the first and second atomization of the feedstock. Usually, water or alcohol, or their mixture is used as a suspension medium (Ref 5). With suspension medium, the surface tension and the resistance against the increased surface area of the suspension fluid during its aerodynamic breakdown also varies. The

aerodynamic breakdown is usually presented by Weber number (We). The liquid breaks up when $We > 12-14$ and deforms into different structures based on their We such as (Fig. 4),

- $We < 100$: bag-like droplets are formed, also referred to as bag break-up regime
- $100 < We < 350$: thin sheets-like structures are formed from the periphery of drops (referred to as stripping regime)
- $We > 350$: the multistage break-up of drop occurs, i.e., catastrophic break-up regime

Alcoholic suspensions, due to their lower surface tension ($\sim 26 \text{ mN/m}$) than the aqueous suspensions (surface tension 38 mN/m), quickly break down during atomization. It was found that the aqueous suspension exhibited a monomodal drop size distribution ($300 \mu\text{m}$) while a broad range drop size distribution ($10-300 \mu\text{m}$) was seen in alcoholic suspensions (Ref 34).

During the secondary atomization, when the atomized droplets of suspensions encounter the heat source, the size of the second breakup droplets decreases due to the droplet fragmentation and solvent evaporation. The resulting particles are greatly influenced by the size of their primary droplets, which in the case of water-based suspensions, are comparatively bigger, and consequently, the velocity of aqueous secondary particles is $70-80 \text{ m s}^{-1}$ higher than the alcoholic suspensions. Moreover, the vaporization temperature also varies with the suspension type, and for water, it is higher ($100 \text{ }^\circ\text{C}$) than the alcohol-based media. Therefore, the energy required to evaporate the liquid

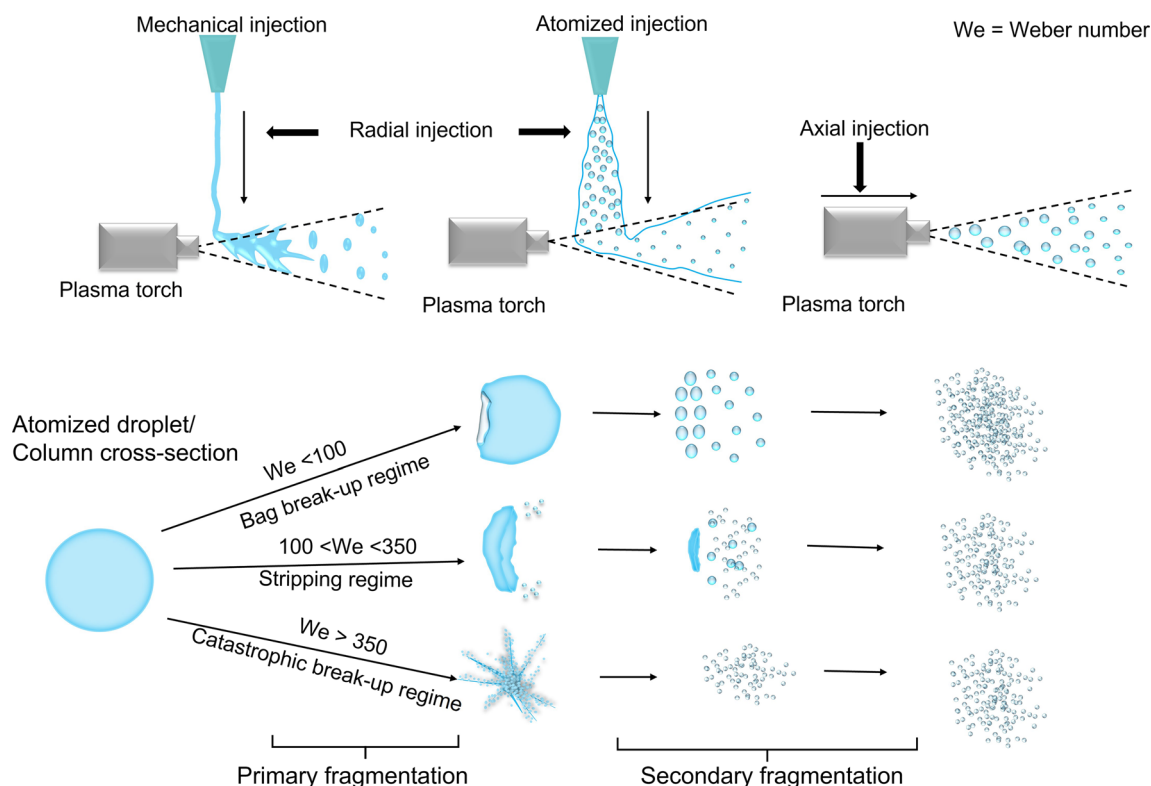


Fig. 4 Schematic representation of the fragmentation of feedstock droplets in the presence of plasma/flame jet based on Weber number (We) value of the liquid feedstock. Inspired by (Ref 36)

during the flight interacting with the heat source is more for an aqueous medium that hinders the efficient melting of the particle (Ref 19, 37).

Generally, suspension medium provides protection to the dispersed particles against oxidation in the presence of flame/plasma by covering them. However, organic solvents due to the exothermic interaction with the heat source, produce additional combustion enthalpy that might affect the dispersed particles adversely. Also, there is a risk of explosion involved in the case of organic solvents. Hence, for technical and safety reasons, water is preferred as a suspension medium in feedstock preparation (Ref 38). However, as we mentioned previously, the in-flight temperature of water suspension droplets is significantly lower due to the high evaporation enthalpy of water (2.26 kJ/g) that cools down the flame/plasma temperature. Sometimes, a combination of aqueous and alcoholic suspensions is used to achieve the desired results (Ref 39).

Solution Precursor Feedstock

For solution precursor feedstock, rather than a colloidal suspension of coating material (particles), precursors of the coating material are used, which during spray, in the presence of thermal energy source, precipitate into the coating material. From injection into the heat source to

hitting the substrate, multiple steps like vaporization, fragmentation, precipitation, sintering, melting and droplet formation take place in a short period (Fig. 2). Hence, sufficient energy is required for coating deposition. Based on the properties of the solution precursor such as surface tension, viscosity, concentration, precursor type, etc. the primary and secondary fragmentation of feedstock droplets take place. Further, due to the interaction with the heat source, precipitation and evaporation take place, leading to the formation of outer crust. After melting of the outer crust, repeated formation and melting of outer crust occur. Based on the thermal and kinetic energy exchange, fully molten, sintered solute and unfragmented hard shells are generated during deposition.

Generally, coatings with low thickness, nanosized porosity and reduced inter-splat boundaries are produced through precursor solutions. Similar to the conventional solution combustion method, particle formation occurs due to the decomposition of metal salts dissolved in a solvent like water, alcohol or mixture. The commonly used metal precursors are butoxides C_4H_9O , nitrates (NO_3^-), acetates (CH_3COO^-), isopropoxides ($-OCH(CH_3)_2$).

Like suspension-based thermal spray, the concentration of precursor also influences the coating microstructures. A higher concentration of the precursor feedstock is beneficial to generate a high volume of droplets resulting in a

dense coating; otherwise, highly porous coatings are obtained. Based on molecular calculations, the final concentration of the solid particles formed from the precursor is calculated. The stoichiometry, precursor type, chemical composition and solvent type affect the coating process and the microstructures (Ref 40).

There are plenty of reports that compare the composition and microstructure of coatings developed using solution precursor feedstock. In a study, acetate-based and nitrate-based precursor feedstocks were compared (Ref 40). The outcome shows that the acetate-based coatings are porous and irregular, having cauliflower-like morphology with plenty of fine re-solidified particles and tiny fully molten droplets attached to the big splats. This could be explained as the carbonaceous organic precursors give rise to exothermic reactions that provide additional thermal energy during flight (Ref 41). This substantial amount of energy facilitated particle formation even at low plasma power (35kW), and the crystallinity of these particles increased with the increased power. Contrarily, in nitrate-based coatings, more uniform coating morphology and well-molten splats with good interlamellar interactions were observed. For nitrate precursors, well-defined particles were formed only at higher plasma power levels (49kW).

It should also be noted that an excessively exothermic process may disperse the oxide particles in the plasma or overheat the substrate (Ref 42). Besides, due to lower surface tension and vaporization temperature, the fragmentation and vaporization of droplets are convenient and aids in efficiently utilizing thermal energy in melting the formed particles before hitting the substrate. It is good to use organic precursors for the oxides that require higher enthalpy for melting, while nitrate-based precursors should be used for comparatively lower energy requirements.

Although solution precursor feedstock does not have particle sedimentation problem, it has its own issue such as pH optimization that limits its potential application. Due to stoichiometric requirements, certain pH is required for the reaction to take place. However, solution with a very low or high pH might deteriorate the hardware (feeder, injector, nozzle, etc.) quality with time, along with introducing impurities during the coating formation. A proper maintenance (for example, cleaning entire route with deionized water before and after spray) could be a short-term solution. Safety is another unavoidable issue for solution precursor thermal spray as due to the hazardous nature of organic solvents, improper storage might lead to catastrophic events. Also, unreacted precursor solution acting as impurity in the coating is another challenge. Hence, it is essential to optimize and understand the role of different parameters involved into feedstock preparation as well as coating deposition.

Hybrid Feedstocks

Feedstocks containing suspended particles into a precursor solution are referred to as hybrid or suspension-precursor or particle-precursor feedstocks. The suspended particles and precipitated particles could be the same or different depending upon the coating requirement. Hybrid feedstock offers an opportunity to gain better control on the coating microstructures by converging the characteristics of suspension-based and solution precursor-based plasma or HVOF spray (Ref 43). Undoubtedly, liquid feedstock-based spray techniques produce fine coatings with nanoscale characteristics, but there is an inevitable need for further improvements to make this process commercially viable. Solution precursor thermal spray coatings, despite having a better control over the coating quality than suspension thermal spray coatings, underperform in terms of deposition efficiency. Hence, hybrid feedstocks are employed to combine the efficiency and versatility (columnar, highly porous or dense, segmented, etc.) of suspensions with stoichiometric control of the solution precursor process.

Hybrid feedstocks produce coatings with unique fine-coarse microstructures that cannot be achieved by other conventional methods (Ref 44). For example, a suspension-precursor hybrid feedstock of ZnO and ZnO/Zn particles produces a coating with a double-layered morphology containing typical clusters and a porous top layer of ultrafine (~ 20 nm) nanograins (Ref 45). Because of having clusters in the bottom layer, the pore size was in microns, while for the top layer, the nanoscale pores were observed due to containing ultrafine grains. These hybrid feedstock-based coatings develop a porous skeleton-like structure, where the dispersed particles melt and act as a binder to assemble the hollow microspheres and crushed shells. Consequently, with improved surface microstructures, optical response and related photocatalytic activities under UV and simulated sunlight irradiation also improved.

Another way of preparing the hybrid feedstock is powder-precursor hybrid feedstocks, where instead of suspensions, conventional powder consumable is simultaneously fed into the flame through another nozzle (Ref 46). In this way, the high deposition efficiency of traditional thermal spray can be achieved along with better control over the chemistry of the coating. Coatings generated by this method are highly dense and show bimodality in particle size. The partially melted, unmelted or re-solidified particles, formed through precipitation of precursor solution are deposited between the interlamellar space of melted dry feedstock particles. This happened because, during flight, particles from powder feedstock melt properly and form a coating over the splats formed through precursor feedstock.

Ideally, to form a well-packed dense coating, an adequate number of nanoparticles should form through precursor solution so that the entire interlamellar space can be occupied. Although researchers have tried to optimize the coating microstructure by calculating the suitable ratio between powder and solution precursor feedstock based on the theory of vacancies (Ref 47), other deposition parameters mainly, standoff distance, need to be tuned in such a way that it is suitable for the melting of powder feedstock as well as particles from precursor solution. It is difficult for the latter, as a quick re-solidification of in-situ formed nanoparticles takes place at higher standoff distances (Ref 48).

Some of the examples of hybrid feedstocks used in liquid feedstock plasma and HVOF spraying are shown in Table 2.

Injection

Injection of the liquid feedstock is the most critical step of the thermal spray coating deposition process, which depends upon the particle size and their velocity and temperature. These parameters affect particle penetration into and interaction with the heat zone. Particles that reach into the core region of the flame/plasma melt thoroughly compared to the particles in the outer area. There are two ways of injecting the liquid feedstock to the core, i.e., through mechanical injection or spray atomization.

In mechanical injection, the feedstock stream is directly (without atomization) injected into the jet with the help of a pressurized reservoir or a pump. The liquid can be fed either directly or in the form of superimposed pulses, generated through a magneto-resistive rod attached to the nozzle, where the velocity of the stream can be varied with the applied pressure (Ref 53, 54). In mechanical injection, it is difficult to control the drop size and their velocity separately as they are correlated and can be fluctuated by varying the pressure or varying the nozzle diameter. If the applied pressure is low, primarily unmelted material will deposit. And if high pressure is applied, there are high chances of obtaining re-solidified particles (Ref 54). Hence, an optimal static pressure, which is influenced by solution properties, must be created for proper deposition. Besides, nozzle characteristics such as diameter, shape and size also affect the injection of feedstock.

In spray atomization, with the help of an inert gas (usually Ar), the low-velocity liquid feedstock is fragmented into spray droplets even before its introduction to the plasma/flame jet. Similar to primary and secondary break-up during flight, this fragmentation also depends on feedstock characteristics, such as viscosity, solid concentration, and surface tension of the liquid. Hence, the

droplet's geometry depends on the Weber number (Section 2.4) (Ref 55). Apart from these, the ratio of the gas flow rate and suspension feed rate ($RGS > 100$) and the relative velocity of gas and fluid also influences the atomization pattern (Ref 56). The droplet size that usually ranges from 2 to 100 μm decreases with the increased RGS value, and sometimes it disturbs the flame (Ref 57). Jordan et al. (Ref 58) designed a homemade capillary injector to reduce the droplet size further (1–20 μm) through transverse atomization. The atomization arrangement also influences droplet size and velocity. For instance, external-mixing atomization produced a liquid jet with 350 μm diameter and 10 $\text{m}\cdot\text{s}^{-1}$ velocity while, internal-mixing atomization produced sprays, varied from a dispersed liquid jet (mean velocity = 20 $\text{m}\cdot\text{s}^{-1}$) to a fully atomized liquid jet (mean velocity = 60 $\text{m}\cdot\text{s}^{-1}$) with a smaller drop size (mean size = 20 μm) (Ref 59).

Suspension/solution viscosity and surface tension also affect the penetration pattern. For instance, aqueous feedstocks are more likely to penetrate the plasma/flame plume than the ethanol feedstocks as they resist fragmentation and secondary break-up due to their comparatively high surface tension. Besides, the high enthalpy of aqueous suspensions/solutions also slows down the vaporization of water. Hence, droplets with a larger diameter and increased mass are formed that efficiently interact with plasma/flame plume due to having high velocity (Ref 60). Likewise, droplets formed from viscous suspensions have high velocity and reach the core region of the plasma/flame by penetrating the jet efficiently, where the solvent evaporates quickly, and the droplet size decreases further (Ref 59).

Effervescent atomization is another way of atomization, in which a mixture of the feedstock and gas is injected into the system, where the pressure difference turns liquid fragments into fine droplets and ligaments (Ref 61, 62). This method is time- and cost-efficient as it generates smaller drops at low injection pressure.

Atomization pressure also influences the droplet formation and their penetration depth into the jet. Droplet penetration improves with the increased atomization pressure, leading to a well-adherent splat formation due to better thermal and kinetic energy exchange in the core region (Ref 63). However, beyond the threshold value any excess pressure gave rise to powdery deposits.

Feeding suspensions into the injector is a complex operation because of the sedimentation tendency of the suspended particles that might lead to clogging. Sometimes, when clogging occurs, the solvent evaporates and the temperature inside the nozzle increases, leading to the formation of a hard crust of agglomerated and sintered particles (Ref 64). Therefore, a constant gas purging is introduced into the injection unit even before introducing the feedstock and after plasma/HVOF jet shutdown to keep

Table 2 Examples of different hybrid feedstocks used in suspension/solution precursor plasma/HVOF spray

Hybrid feedstock type	Coating material	Coating deposition	Particle size (µm)	Coating thickness (µm)	Porosity (%)	Reference
Powder (YSZ) + Solution precursor (zirconium acetate and yttrium nitrate hexahydrate)	YSZ	Layer-by-layer APS + SPPS & simultaneous APS + SPPS	125	250	~12	(Ref 49)
Hybrid powder (7YSZ) + solution precursor (Si(OH) ₄)	SiO ₂ + ZrO ₂	High-velocity plasma spray	5-22	10-20	...	(Ref 50)
Powder (T-400) + Suspension (Cr ₃ C ₂)	carbide-laden T-400	SPS (axial)	Powder (45) + Suspension (40 wt.% of 3.8)	100-200	5-6	(Ref 51)
Powder (Ta ₂ O ₅) + solution precursor (Ba acetate/nitrate, Mg acetate/nitrate)	Ba(Mg _{1/3} Ta _{2/3})O ₃ (BMT) Perovskite	SPS + SPPS	Powder (5)	7.69 (acetate-based precursors) & 11.97 (nitrate-based precursors)	...	(Ref 40)
Powder (Al ₂ O ₃) + YSZ solution precursor (yttrium(III)nitrate hexahydrate+zirconium acetate+ acetic acid)	Al ₂ O ₃ -YSZ/ZrO ₂	HVOF (suspension + solution precursor)	Powder (25) + precursor formed particle (< 0.2)	(Ref 47)
Powder (Inconel 625) + suspension (Cr ₃ C ₂)	IN-625 + Cr ₃ C ₂ hybrid	HVAF (powder + suspension)	Powder (-30 + 10) & Cr ₃ C ₂ (4)	~300	<3	(Ref 52)

the nozzle clean and cool. In 2011, Cotler et al. (Ref 65) developed a cleaning device that purged a small amount of liquid (in the form of mist) mixed with the gas, which helped cooling and cleaning the nozzle.

Another type of injector was a liquid-in-gas injector, in which the diameter of the inner liquid bearing tube was decreased adjacent to the outer gas carrying tube that helped save the energy and cost by reducing the required pressure supplied by the pump (Ref 66). Moreover, vanes attached to the periphery of the inner tube helped focus the gas flow at the exit of the nozzle. Using a vibrator could also help limit the solid plug formation and separate the large agglomerates from the suspension (Ref 67).

Various suspension feeders are developed for feeding, and the widely used commercial feeders are NanoFeed™ Liquid & Suspension Feeder (Northwest Mettech Corp., North Vancouver, BC, Canada) and pressurized suspension feeder (Fraunhofer IWS) (Ref 35, 68, 69). Besides, different homemade and industrial atomizers are also available for feedstock injection (Ref 15, 70).

Based on the assembly of injectors, the injection can be categorized into two parts, i.e., radial and axial (Fig. 5).

Radial

In radial injections, the feedstock is introduced to the flame/plasma from the outside (of the gun). This is a widely employed injection route for plasma spray, where the position or the angle of injection can be varied as per the required material (from ceramic to polymers). Droplets in the core region of plasma have different properties than the peripheral zone, and in which region droplets are going to be formed is mainly decided by the penetration depth of the injected feedstock into the plasma jet and its velocity. Regardless of the injection method, for successful penetration of feedstock into the jet, the momentum density of droplets ($\rho_l v_l^2$; where ρ_l is the specific mass of the liquid droplet and v_l is its velocity) must be higher than that of the plasma jet at the injection point. A numerical study on suspension injection shows that the penetration depth of the feedstock increases with its injection velocity but up to a specific value (Ref 71). Beyond that, inefficient melting of particles takes place due to their reduced dwell time in the flame.

Injection position also affects droplet formation. If the axial distance between the torch and nozzle exit is smaller along with a reduced injection angle (toward the gun), feedstock's penetration depth increases, and consequently, the temperature and velocity of the particles also increase (Ref 71). Even though radial injection in HVOF is quite rare, recently, the effects of radial injection dynamics and feedstock interaction with HVOF flame were studied to deposit the heat and oxygen-sensitive materials (Ref

70, 72). In a study, graphene nanoplatelets were deposited using the radial injection of feedstock in HVSFS that showed that with the increased flame power, the temperature and velocity of graphene nanoplatelets (GNPs) increase and decrease with the feedstock flow rate increment (Ref 70).

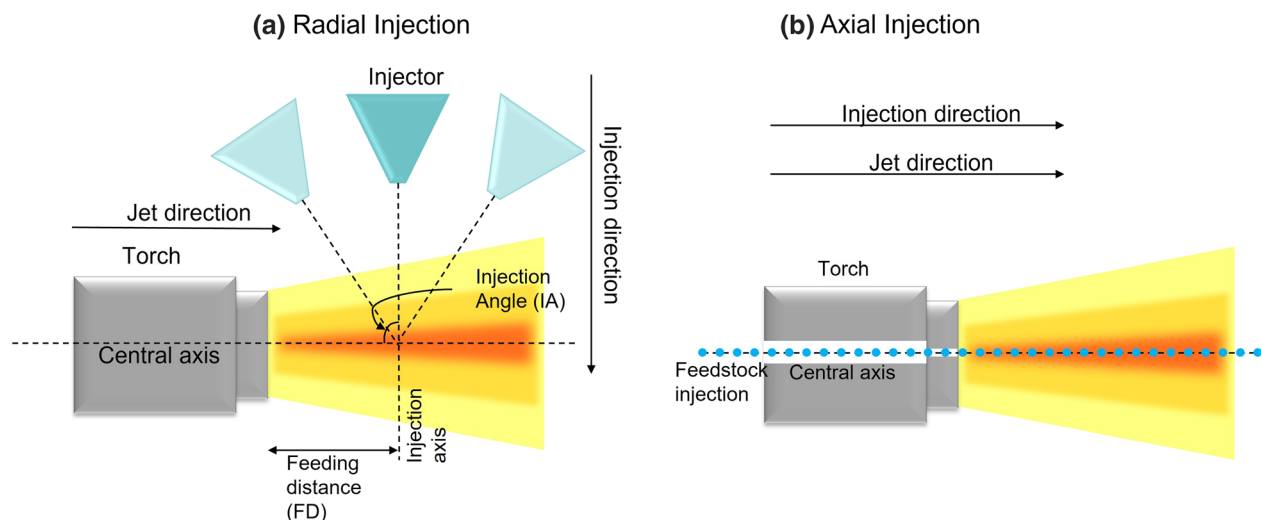
The radial injection is also suitable for solution precursor-based thermal spray, which provides control over the degree of pyrolysis through injection parameters. For example, in the case of thermal barrier coatings (TBCs) where semi-pyrolyzed material that forms beneficial vertical cracks is favored, radial injection allows more droplet formation into the colder (outer) zone and increases the probability of formation of desired coating microstructure (Ref 57). Sometimes, due to the perturbation, the injected feedstock does not interact well with the flame. Hence, inefficient energy transfer between suspension droplets and torch occurs, leading to the insufficient melting of particles. To resolve this issue, multiple-feed injectors located in a circle centered at the torch axis are designed to allow the deeper penetration depth and could be used to inject multiple suspensions simultaneously (Ref 73).

The radial injection provides the freedom of controlling the coating microstructures by changing the injection position and angle. However, some challenges, such as inefficient heat and momentum transfer between jet and droplets, the inadequate velocity of fragmented droplets, and the need to optimize the injection position and angle, are attached to it. This type of injection is suitable for certain situations where oxygen-sensitive material (graphene, CNT and fullerene) needs to be deposited because the short in-flight time reduces the probability of degradation.

Axial Injection

In the axial injection, the feedstock is directly introduced into the torch or the combustion chamber, where additional atomization of the feedstock before interacting with the plasma/HVOF jet takes place. Because of the longer dwell time within the plasma/HVOF jet and complete entrapment of feedstock, an improved thermal and momentum exchange between feedstock droplets takes place that helps in improving the coating deposition efficiency (Ref 35). The axial injection is considered energy- and cost-efficient as it requires comparatively low operating power to melt the particles due to better thermal and kinetic energy exchange.

In axial injection, suspension characteristics such as surface tension and viscosity affect the fragmentation differently than the radial injection (Ref 35). For instance, the fragmentation of feedstock droplets for ethanol-based Y_2O_3 suspension with solid content 0.1–4 vol.% was so



$0^\circ < IA < 90^\circ \rightarrow$ Poor energy exchange between droplets and plasma/flame
 $90^\circ < IA \rightarrow$ Better energy exchange between droplets and plasma/flame

Injection Angle (IA) = $0^\circ \rightarrow$ Good energy exchange between droplets and plasma/flame

Less FD \rightarrow Good energy exchange between droplets and plasma/flame
 More FD \rightarrow Poor energy exchange between droplets and plasma/flame

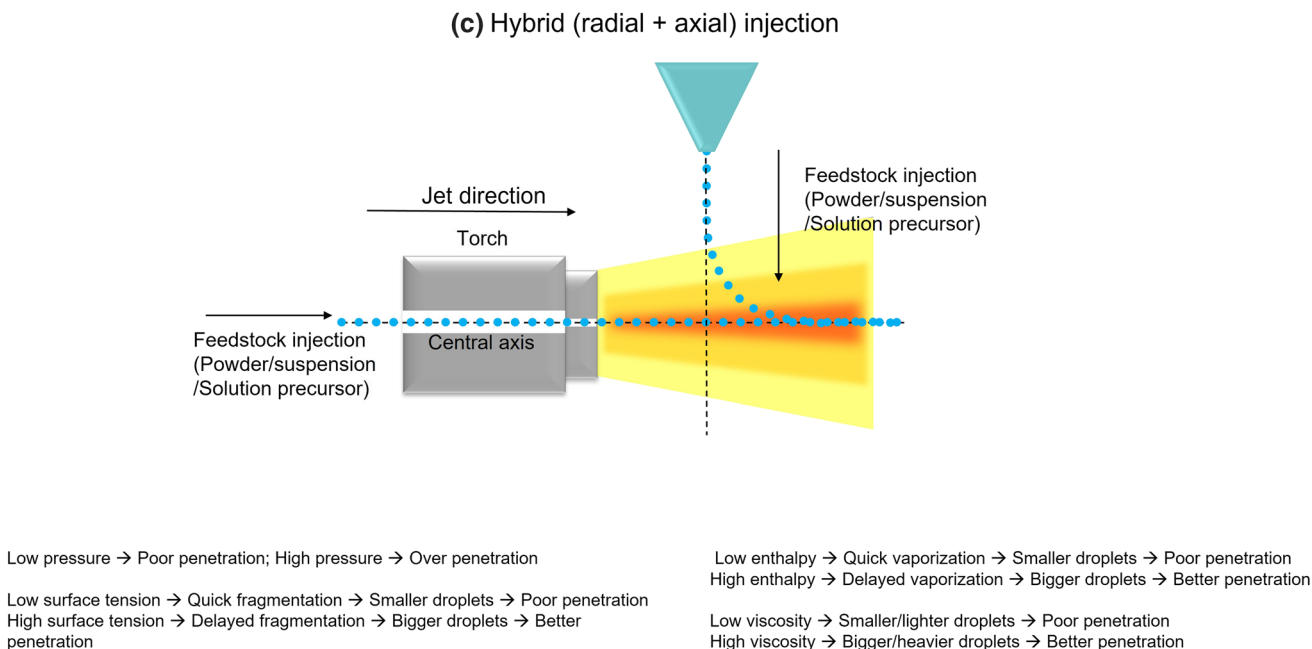


Fig. 5 Schematic representation of (a) radial, (b) axial and (c) hybrid injection of the feedstock into the plasma/flame jet during plasma/HVOF process

severe that the size of molten droplets was unaffected by the initial droplet size and the solids concentration in the initial droplet (Ref 23). However, the size distribution of powder in the suspension significantly impacts the diameter of the molten droplet. When axial injection occurs at 0° angle with the flame in S-HVOF, due to the same direction of travel, the interaction between feedstock liquid and flame becomes very limited, and hence, large suspension droplets are formed. Besides, the torch temperature also

decreases significantly due to the vaporization of the solvent (Ref 74). For an efficient injection, the injection angle value needs to be optimized according to the feedstock properties and torch design. For example, in one such study, Mahrukh et al. found that the suitable injection angle for their feedstock was 10° - 15° (Ref 61). At an angle lower than this (5° - 10°), poor evaporation of feedstock droplets took place, and chances of droplets exiting the torch without evaporation increased. If the injection angle was

increased (15° – 20°), a collision between droplets and the combustion chamber increased that might deteriorate the torch by depositing on the internal wall.

For hybrid injection, a unique arrangement of dual or triple feeders is used, where each feeder is controlled independently to get the desired coating architecture, each feeder is controlled independently to get the desired coating architecture (Ref 75–77). Through this setup of feeders, composite, layered or graded coatings can be obtained. Based on the assembly of the feeders, this could be categorized into radial, axial or mixed types of injection (Ref 43, 78).

Torches

Plasma Torches

Torches with the cylindrical cathode (with power <45kW) are used for the powder-based spraying. In a recent scenario, guns with a high-enthalpy plasma source were used to aid proper evaporation of solvent before powder melting due to the exchange of more kinetic and thermal energy to the particle droplets. The characteristics of plasma jet such as plasma source gases and their velocity, plasma power and electrode design are the variables that control the morphology and deposition efficiency of coatings. As mentioned, the momentum density of the feedstock and plasma jet influence the injection and fragmentation of the feedstock stream, and the momentum density of plasma depends on the mass density of plasma gas/es and plasma gas/es velocities. Therefore, with power, the plasma velocity increases, and consequently, acceleration and heat transfer to the droplets also increase.

A negative aspect of the conventional high-power plasma torches is that with time, erosion of anode occurs due to the arc root fluctuations, diminishing the voltage along with the momentum and heat transfer to the feedstock. Voltage fluctuation is represented by the ratio of the difference between the maximum and minimum value of the voltage during fluctuation (ΔV) and the mean value of voltage (V). To increase the plasma power or, in other words, to reduce/control the voltage drop, a small amount (< 5 vol.%) of other gas/es such as He, H₂, or N₂ is mixed with Ar. It was found that mixing H₂ with Ar in comparison to the He offers more power and more voltage fluctuations (Ref 79).

Water-stabilized plasma (WSP) is also used to satisfy the need for a higher power plasma source. According to Hrabovsky's study (Ref 80), WSP torches produce considerably higher plasma enthalpy (up to 272 MJ/kg) and plasma velocity (6000 m/s) compared to the conventional gas-stabilized plasma (GSP) torches (enthalpy up to 25 MJ/

kg and velocity up to 2000 m/s). In WSP, H₂/O₂ plasma is generated due to the ionization of the steam, and the high content of H₂ creates the plasma jet with high plasma temperature and flow velocity (Ref 80, 81). Mušálek et al. (Ref 82) utilized the advantages of WSP by using WSP[®]500 (Institute of Plasma Physics AS CR, v.v.i., CZ) to deposit the SPS-based YSZ coatings. They found that all the coatings exhibited columnar cauliflower microstructures with segmented cracks on the free surface, irrespective of their spray conditions. WSP torch, even after the in-flight agglomeration of particles, generated (~ 1 or 2 times) smaller splats than the GSP. The most important feature of these liquid-stabilized high-enthalpy torches is that they improve the deposition efficiency (> 50%) by supporting the high feedstock throughput, which is more than 100 ml/min (Ref 81–83). These torches are well suited for cost-effective industrial-scale applications as no helium is required for plasma generation.

Recently, a hybrid-WSP torch (WSP[®]-H 500) has been developed, in which benefits of water vortex are converged with the gas vortex. In WSP-H, at first, GSP (argon-based) is generated, followed by combining with the WSP in the water-stabilized section, increasing the plasma enthalpy (up to 300 MJ/kg), flow velocity (up to 7000 m/s) and plasma density (up to 9.8 g/m³) (Ref 84). Besides, the WSP-H torch creates a plasma jet with a longer plasma path, which prevents the deceleration and cooling of the in-flight particles before hitting the substrate, even at the longer stand-off distances (for example, 90 mm 100 mm SOD) (Ref 60). The deposition efficiency of WSP-H torch-based coatings can be further enhanced by introducing an additional feeder (dual or triple feed) injection setup. These characteristics make WSP-H torches a promising option for high-enthalpy plasma sprayed coating used for large-scale applications.

Multi-electrodes systems are also used to limit the arc root fluctuations and increase the enthalpy of the plasma gun. One such example is the Triplex I and IITM (from Oerlikon-Metco) DC torch, in which a cascaded plasma arc is generated by using three independent cathodes and a common anode, producing three isolated arcs. Hence, the plasma power increases along with reduced voltage instabilities, generating a more extended plasma jet (up to 55–60mm) than the conventional torches (<50mm).

Axial III (from Northwest Mettech Corp.) is used extensively to support the axial injection of feedstock (especially for particles with a high melting point). It also contains three different cathodes, but unlike Triplex, three separate anodes cumulatively generate 30–150kW plasma power and 300–500 m/s plasma velocity. Therefore, due to high enthalpy and better plasma stability, this torch more efficiently transfers the heat and momentum to the particles. The feedstock is introduced axially between these

three different sets of electrodes through a water-cooled nozzle in this setup. Recently, Aeroplasma Corp., Japan, has developed a twin-cathode type plasma spray gun (Ref 85) that contains three plasma torches: one with reversed polarity (called as P-torch) and two sub-torches with normal polarity (referred to as N-torches), generating a hairpin-shape plasma jet during operation. The unique quality of this torch is that it deposits coating at low power and gas consumption and is suitable for both radial and axial injection.

The radiofrequency inductively coupled plasma (RF-ICP) torches are also used to deposit SPS/SPPS coatings that feed the suspension axially and are considered suitable for depositing the refractive materials such as Barium Magnesium Tantalate (BMT) due to their longer dwell time (Ref 86). RF-ICP torches work at reduced pressure (15 kPa) and generate a more extended plasma jet (~70 mm). The PL-50 (Tekna Plasma Systems Inc., Sherbrooke, Canada) is the commercially available RF-ICP torch.

S-HVOF Torches

Axial injection of the feedstock is commonly used in S-HVOF, where the feedstock is introduced directly into the torch's combustion chamber (injection pressure 0.3–1 MPa). Because of the low temperature of the HVOF flame compared to the plasma plume and additional temperature cooling due to the vaporization of the solvent, axial injection is highly preferred so that efficient energy and momentum can be transferred between the energy source and feedstock droplets.

Various modifications have been done in the conventionally used HVOF torches to support the internal injection of feedstocks. The TopGun-G (GTV mbH, Luckenbach, Germany) and Diamond Jet Hybrid (Oerlikon Metco, Wohlen, Switzerland) torches are widely used to deposit suspension-/solution-based HVOF coatings (Ref 87). TopGun-G torch contains water-cooled gas distribution, combustion chamber, and nozzle tube, along with supporting a wide range of fuel gases such as propane, acetylene, or hydrogen. Using acetylene as fuel is beneficial for depositing the material with a high melting point as it generates the highest flame temperature (Ref 88). Diamond Jet Hybrid is made up of a hybrid system of the water-cooled chamber and the attached extended nozzle. Generally, premixing of fuel and oxygen is preferred before injection.

The thermal power of a torch fluctuates with various parameters such as flow rate, fuel/oxygen ratio, fuel type, solvent type, design of combustion chamber unit and feeder type (Ref 19, 87, 89). Killinger et al. (Ref 87) studied the effects of different kinds of feeders and their nozzle size and found that feeding through a pressure vessel operated with compressed nitrogen gas with a smaller nozzle

diameter exhibits efficient melting of particles. Usually, a longer expansion barrel attached to the combustion chamber is preferred as it allows complete evaporation of the solvent and proper melting of particles due to longer dwell time, producing comparatively denser coatings (Ref 90).

Sometimes, due to the turbulent flow of the fuel gas, the deposition of droplets on the chamber wall and injector nozzle takes place, which creates defects in the coatings due to the occasional protrusion of these large particle deposits. Also, due to the inefficient vaporization of solvent in the low-velocity region of the combustion chamber, chances of defects in coating increase. Variation in the design of the combustion chamber is done to avoid these issues. For instance, conical-shape chambers are preferred to deposit low melting point materials such as hydroxyapatite, while cylindrical-shape nozzles are used for high melting point materials (Ref 1).

Most of the S-HVOF reports are based on gas-fueled torches rather than liquid (kerosene)-fueled torches as the varied quality of kerosene complicates their atomization and combustion. A comparatively longer combustion chamber is designed for liquid-fuel torches to support their prolonged combustion time. The feedstock is injected radially between the combustion chamber and the expansion barrel, where gas temperature decreases (<3000K) but the velocity is higher (2 km/s). The longer expansion barrel provides droplets the opportunity to get sufficient heat inflight (Ref 33, 91). In this case, although the transferred enthalpy between particles and the flame is lesser than the gas-fueled torches, kinetic energy is higher.

Fuel to oxygen ratio in the chamber is another crucial parameter affecting the coating quality. The oxygen-rich mixtures give rise to longer flames, while fuel-rich mixtures produce coatings with less oxide content (Ref 92). Moreover, to increase the enthalpy, ethanol-based or mixed ethanol-water suspensions are used. If the oxygen content is not enough in the premixed fuel/oxygen mixture, ethanol droplets do not combust properly because the vaporization of ethanol occurs in the middle of the combustion chamber where only leftover (from premixed combustion) oxygen is available for the reaction (Ref 1). Hence, it is essential to decide the mass fraction of fuel and oxygen before combustion (Ref 19). Apart from the axial injection of fuel and feedstock, a combination of axial injection of fuel and radial injection (inside the combustion chamber) of feedstock is also used.

Coating Deposition

Role of Surface Roughness

The surface roughness of the substrate significantly influences the coating morphology by introducing the

nucleation sites and providing anchoring points. It is evident from the previous studies that a rough surface produces coatings with columnar microstructures due to the deposition of molten/semi-molten droplets on asperities (Ref 93–96). In case of thin coatings, the surface irregularities are reproduced, and the shape of rough surface is still visible due to less depositing material.

With the increased roughness (arithmetic mean of roughness (Ra), root mean square roughness (Rq) and mean roughness depth (Rz)), the coating becomes more irregular, and its microstructure shifts from vertical cracks to columns (Ref 93). Hence, it is quite difficult to obtain smooth coatings on a very rough surface. It happens when a perpendicular plasma jet carrying the particle droplets hit the substrate, only big particles with a high moment of inertia hit the substrate perpendicularly, while particles with a small diameter are easily influenced by the drag force of the plasma trajectory and get carried away from their original direction, hitting the substrate at a shallow angle. On a rough surface, small droplets deposit on the nearest asperities giving rise to the columnar structures (shadowing effect), which start growing vertically and horizontally (cone-shape) with coating thickness. Inter-columnar voids separate these columns, and the head of columns exhibit a typical cauliflower-like morphology.

For the smooth surfaces (e.g., mirror-polished), fine droplets travel parallel to the substrate without any hindrance and deposit at the far range (no shadow effect). Generally, smooth surfaces produce dense coatings with less crack density. However, with the increased coating thickness, the previously deposited splats/particles on the smooth surface start acting as newly formed asperities, which obstruct the path of subsequent particles. Once the roughness reaches a particular value, the crack appears, meaning cracks do not emerge from the interfacial region (throughout the coating thickness), instead develop after a certain coating thickness. In short, it could be generalized that the smooth surfaces produce comparatively more continuous and uniform coatings with lesser crack density. Contrarily, rougher surfaces generate porous, columnar, and more irregular coatings.

Grit blasting, grinding, polishing, and laser treatment are the commonly used methods to control the surface topography. Zhao et al. (Ref 93) have compared the Vickers hardness of the coatings obtained on the mirror-polished ($R_a = 0.04 \mu\text{m}$), grit blasted (low pressure ($R_a = 0.16 \mu\text{m}$) and high pressure ($R_a = 3.51 \mu\text{m}$)) and ground surface ($R_a = 1.05 \mu\text{m}$), and found that the hardness decreased with the increased roughness. According to Sokolowski's report (Ref 97), coatings generated on a laser-treated substrate ($R_a = 3.6 \mu\text{m}$; $R_z = 17.6 \mu\text{m}$) exhibited a unique 'peak-and-valley' microstructure, where each peak gave rise to a separate columnar structure, and the valley formed a

longitudinal pore. Besides, the grain/splats formed over the peaks were round and comparatively smaller in size than the splats in the valley area. The generated coating was regular in pattern and twice as rough ($R_a = 7.4 \mu\text{m}$; $R_z = 43.5 \mu\text{m}$) as the substrate. With the increased solid content in the suspension feedstock, the columnar structures become less visible, possibly due to the increased density of the coating running along the length of the substrate (Ref 96).

Role of Substrate Preheating

In thermal spray, the temperature of the substrate influences the solid-liquid interactions (flattening i.e., splash mechanism, solidification and adhesion) between the substrate and the molten particles (Ref 98). For example, if a substrate is preheated (substrate temperature, T_s) above its transition temperature (T_t , the temperature beyond which disk-shaped splats are formed instead of splash), the desorption of the surface impurities (dirt/grease) takes place, allowing a better substrate and molten metal droplet interaction (better wettability) during thermal spray. On the contrary, a non-preheated (at room temperature) substrate exhibits reduced interfacial interactions due to the rapid vaporization of the adsorbents upon the impact of hot molten droplets (Ref 99). Sometimes, the rapid evaporation of adsorbents modifies the final shape of splats by lifting off its parts from the substrate (Ref 100).

Besides, preheating amends the topography of the substrate that ultimately influences the splat formation. Cedelle et al. (Ref 99) preheated the mirror-polished stainless steel substrate above its transition temperature (at 673 K). They found that the roughness of the oxide layer has increased with positive skewness (S_k), which reduced the droplet flattening time by half and at least doubled the cooling rate (more for nanosized droplets). Moreover, the preheated substrate gives rise to a disk-shaped splat, while the non-preheated substrate forms splash-shape splats. It could be explained as when a molten droplet hits the substrate, ridges of the deformed substrate hinder the splat expansion. These ridges result from friction between the slightly melted substrate surface (including the formed oxide layer) and the molten droplet, and later due to the homogenous and faster cooling, a disk-like splat is formed (Ref 101).

With the increased substrate temperature, the flattening ratio of splats (splat size/drop size) decreases. However, the splashing of splats re-occurs with the increase in substrate preheating duration due to the re-adsorption of gas/condensation, which results in poor wettability (Ref 102). Similarly, the preheating temperature significantly impacts the interfacial bonding between the splat and the substrate. A modeling study (Ref 103) proves that the glass

transition temperature is the intrinsic bonding temperature required for a perfect bonding at the substrate-splat interface.

Many reports state the effects of substrate preheating on the coating microstructures formed through a liquid-based thermal spray. Although smaller splats are formed through SPS/SPPS/HVFSF than the powder-based spray, the substrate preheating has similar outcomes (Ref 93). It was found that the coatings formed on the non-preheated substrate exhibited an increased number of horizontal cracks due to the weak substrate-splat interfacial interactions. Further, at 150 and 300 °C, narrower and no visible cracks were observed, respectively (Ref 93).

Substrate preheating influences the crystallinity and grain size of the coating. Tarasi et al. (Ref 104) found that a preheated (at 350 °C) mild steel substrate produced Al-YSZ coatings with higher amorphous content and a smaller grain size. According to Wang et al. (Ref 105), a splat formed at preheated substrate can be divided into three zones: coarse grain zone (central), medium grain zone (transitional) and fine grain zone (peripheral). Also, the area of these grain zones varied with the substrate preheating temperature, where area % of central coarse grain zone increased and area % of peripheral fine grain zone decreased with the increased temperature from 100 to 350 °C. Also, they found that during solidification, if the preferred growth direction of fine grains is parallel to the heat extraction direction, they exhibit the fastest growth.

Role of Substrate Shape

Obtaining a uniform coating on a curved substrate remains a challenge for various industries. Hence, it is essential to understand the role of the shape of the substrate in affecting the coating microstructures. According to Caio et al. (Ref 95), the coating thickness decreases with the decreased radius of curvature. It happens because the finer particles following the gas streamlines were dragged away from (parallel to) the substrate, and hence, lesser material was deposited. The particles hitting the flat substrate were 1.3 times and 2.9 times more in numbers than the cylindrical and rod-shaped substrates, respectively. According to a numerical study (Ref 106), the number of particles hitting the flat substrate was 2.3 times more than the curved ones.

The difference in the number of particles hitting the substrate in these two studies could be attributed to the mismatch between the plume and the substrate's central axes. In the latter, most of the particles were traveling above the torch axis, while in Caio's study, particles were equally distributed in both directions.

A new parameter (catch rate) is defined to represent this,

$$\text{Catch rate}(\%) = \frac{\text{Mass of landed particles in } \Delta t \text{ time}}{\text{Mass of injected particles in } \Delta t \text{ time}} * 100$$

The curved surfaces exhibited well-defined columnar structures as compared to the flat ones (rod shape > cylindrical > flat substrate) because of particles hitting the substrate at shallow angles (between 10° and 20°). Particles traveling toward the curved substrate above 10°-20° angles passed the substrate without hitting it (Ref 106). Because of shallow impact angles, the column width decreased with the increased distance from the center (Fig. 6) (Ref 95).

Coating Architecture

The coatings produced using liquid feedstock exhibit different kinds of nano- and micro-scale features such as vertical cracks, lamellar or columnar structures and pores, depending on various spray parameters.

Columnar coatings: The formation of the columnar structure is widespread due to the deviation of the finer particles from the flow trajectory. VanEvery et al. (Ref 16) compared the microstructure variation in the coatings deposited by using microsized (D50 μm) and nanosized (D80 nm) particles-based suspension feedstocks. They found that micro-sized particles produced a coating with lamellar structures because they are big enough to be influenced by the plasma drag force. Consequently, instead of depositing only on substrate asperities, the splat formation takes place on the entire surface in a comparatively homogenous manner, forming lamellae. On the contrary, the nanosized particles give rise to the columnar structures due to the shadowing effect. According to the column development theory, the coating morphology can be categorized into three regions. First, the initial area, where the column is not defined clearly, second, where the column starts exhibiting a cone-shape feature and separates to the other column with inter-columnar voids and at last, the top region, which introduces typical cauliflower-like features to the coating (Ref 94). The normal and vertical characteristics of substrate asperities influence the column length and width associated with the column mean diameter and coating thickness, respectively. The mean diameter of a column exhibits a linear dependency on the coating thickness.

Multilayer or graded coatings: Hybrid (powder + suspension/solution feedstock) thermal spray processing is a facile method that provides an opportunity to obtain coatings with three possible architectures: layered, composite, and graded. Layered and composite structures take place due to the sequential and simultaneous feeding of the feedstocks, respectively. While the concurrent feeding of the powder and suspension/solution feedstock with a varied

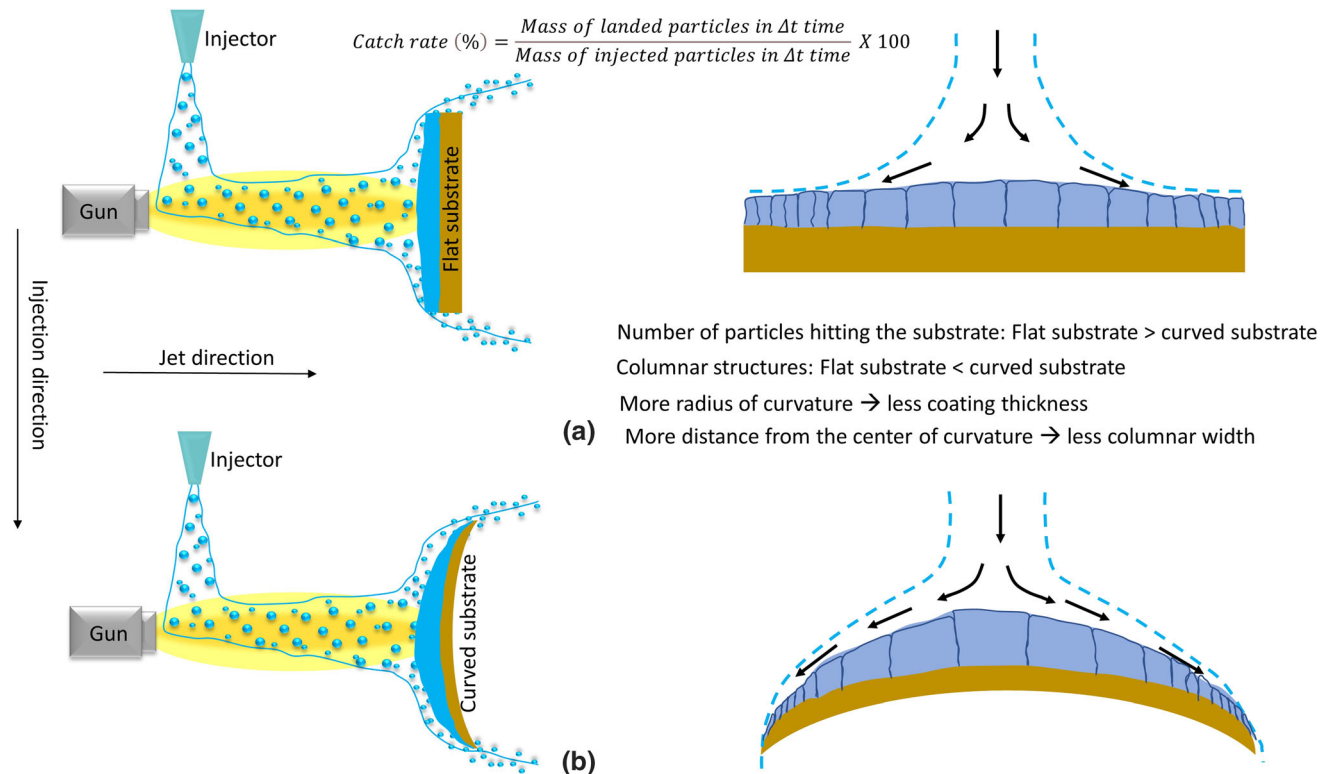


Fig. 6 An illustration of the effect of substrate shape coating deposition and microstructure: (a) for flat substrate and (b) for curved substrate. Inspired by (Ref 95)

relative feed rate of one or both produces graded coatings (Ref 43). The performance of these hybrid coatings can be controlled by altering feedstock properties and their related parameters. Aghasi-beig et al. (Ref 107) varied the electrocatalytic activity of the layered (APS+SPPS) coatings by varying the number of passes (3, 6, and 10) of SPPS coating sprayed on the top of APS coating and found that the coating with six thermal spray passes of SPPS exhibited the highest electrocatalytic activity due to the hierarchical coating microstructures with improved surface roughness ($S_a = 14.4 \mu\text{m}$). Composite coating architecture converged the lamellar features of powder feedstock-based coating with the unique microstructural features such as nanosized pores, cauliflower-like surface, etc. of liquid feedstock-based coatings (Ref 49). Similarly, a porous skeleton-like ZnO-ZnO coating with unique features was formed by Chen et al. (Ref 45) through the hybrid (SPS and SPPS) process. Functionally graded architecture is highly preferred in applications such as TBCs (Ref 108). TBCs sometimes suffer from delamination of the topcoat from the bond coat that diminishes the coating durability. In this case, graded coatings could be beneficial, providing a graded interface with a lesser mismatch in thermal properties rather than a typical distinct interface, delaying the coating failure by resisting the crack initiation and propagation into the high toughness near-interfacial region (Ref

109, 110). Hence, TBCs with improved furnace cycle durability and low thermal conductivity can be achieved using graded architecture. Besides, nano features introduced into the interfacial region aid in reducing the oxygen activity, and consequently, reducing the rate of formation of the thermally grown oxide (TGO) (Ref 111). To gain a more accurate understanding of functionally graded coatings, Ai et al. performed a numerical study (Ref 112) and found that the magnitude of deposition stress in functionally graded coatings was lower than the conventional coatings, varying with the coating and substrate thickness.

Doping is another route for homogeneously intermixing materials in the coating architecture that can be achieved by deposition of intermixed suspensions, precursor solutions or hybrid (powder + suspension/precursor solution) feedstocks. Doping provides compositional control and more proximal contact between the dopant and matrix. However, proper understanding of possible interactions between additional material and matrix, giving rise to intermediate species is necessary. Solution feedstocks are more preferred over suspensions for doped coatings due to their better control over stoichiometry and intermixing of constituents.

To engineer the desired hybrid/graded/doped coating architecture, it is essential to optimize the spray parameters that are fit for powder and precursor solution/suspension,

which could be critical due to the subsequent in-flight processing of powder-based and liquid-based feedstocks.

Cost Assessment of Suspension/Solution Precursor Plasma/HVOF Spray

The capital expenditure covers the investment done in advance and is a combination of the cost of various things such as land, plant and equipment and associated installation, training, and any other cost essential to get things up and running (Fig. 7). The operational cost includes the expenditures related to the rent and utilities, wages and salaries, audit/maintenance fees, overhead and administrative expenses, and the running cost of consumables (Fig. 7).

Capital Expenditure (CapEx)

A typical plasma or HVOF spray equipment contains fundamental parts such as a plasma/HVOF gun, injection nozzle, feeder pump, heat exchanger, controller with a 6-axis robotic arm, and turntable. Hence, the cost of these parts comes under equipment cost. Apart from the equipment cost, an installation charge is also added to capital expenditure. For safety purposes and reducing contamination possibilities, a separate spray booth is required for thermal spray. For instance, during HVOF spray, the noise level is around 123 dB, and hence, an acoustic

(soundproof) room with a monitoring system and flow controllers is essential. Besides, an additional cost of an extractor (for health and safety purposes) is also added to the initial investments.

After setting up a spray booth, installing gas (for combustion or plasma)/fuel cylinders and related regulators further increases the initial cost. To evaluate the coating morphology, diagnostic equipments are also required, and the cost of the diagnostic equipment increases with the complexity of the process. For example, spray of feedstock with nano or submicron particles needs more complex diagnostic tools as compared to the powder feedstock spray. Besides, if instead of commercial liquid feedstocks, laboratory-made feedstocks are used for the thermal spray, additional investment for laboratory setup and related equipments is also required.

The total equipment cost varies with the choice of core components as per the requirements. For instance, atomizing an injection nozzle (ultrasonic nozzle) instead of a simple injecting nozzle increases the equipment cost. The choice of plasma guns or HVOF combustion chambers affects the total equipment cost and influences the operational cost by manipulating the deposition efficiency. For instance, the Triple-Cathode spray gun (Oerlikon Metco Ltd., based on the Cascading Arc Technology) provides high voltage levels with low current input (up to 90 kW power capacity). It can also be used in extended spray operations without the need for the replacement of core gun elements. Also, it provides benefits of high material throughput, which ultimately reduces the operational cost. According to Oerlikon Metco’s report (Ref 113), the TriplexPro-210 spray gun saves 24% and 27% cost compared to the Metco 9MB series and Metco F4 series, respectively.

Although some of the existing spray guns, such as the Praxair SG-100 gun can be used for liquid suspension injection (predominantly for radial injection), a large selection of spray guns solely dedicated to liquid feedstocks is provided by Oerlikon Metco Ltd. Table 3 shows spray guns and feeders available at Oerlikon Metco Ltd.

Apart from the Oerlikon Metco, other companies such as GTV GmbH, Luckenbach, Germany, Northwest Mettech Corporation, Vancouver, BC, Canada, Praxair, Progressive Surface, Metallizing Equipment Co. Pvt. Ltd., and Miller Thermal Inc. (Wisconsin, USA) provide equipment, components and services for liquid feedstock thermal spray.

Operating Expenditure (OpEx)

Operating cost of suspension/solution precursor plasma/HVOF spray varies with different components such as spray gun model, injection type, feed rate, deposition efficiency, and spray method for thermal spray. For example, buying nanomaterial suspensions could increase

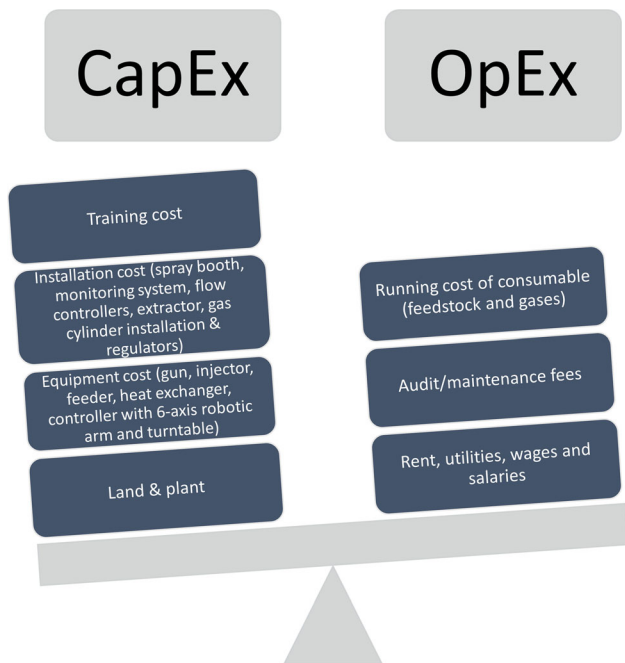


Fig. 7 Representation of CapEx and OpEx related to SPS, SPSS and S-HVOF spray

Table 3 Commercially available thermal spray guns and feeders designated to the liquid feedstocks by Oerlikon Metco Ltd

Components	Models
Plasma torches	TriplexPro-210
	SinplexPro series
	F4MB-XL series
	Metco 9MBM
HVOF torches	Diamond Jet Hybrid
Feeders	LFS 400 Liquid Suspension Feeder

the total operational cost, and if the feedstocks (suspension or solution precursors) are prepared in the laboratory, addition cost for the laboratory setup, consumables, and storage is required.

Deposition efficiency (DE) plays a significant role in dictating the coating cost. For example, if a spray process has a very low DE, probably a greater number of passes would be required to deposit the desired coating thickness, which ultimately increases the cost. The axial injection is considered more efficient due to better thermal and kinetic energy transfer in terms of DE. In radial injection, sometimes the smaller droplets cannot enter the core region of plasma/flame and deflect from their path, which leads to insufficient energy transfer, and hence, poor deposition occurs. The axial injection is quite common in the S-HVOF process compared to the SPS/SPPS, making S-HVOF a high throughput method. Even though solution precursor-based feedstocks provide better control over the chemistry and microstructures of the coating, due to the complexity, low deposition efficiency and comparatively high operational cost, they are still not used at the industrial level.

DE also depends on the SOD, and it decreases with increasing SOD (Ref 114). Moign et al. (Ref 115) performed the life cycle assessment (LCA) of APS, SPS (axial and radial) and SPPS, where, based on previous studies, they considered DE as 60% (APS), 50% (for axial SPS), 30% (for radial SPS) and 30% (for SPPS).

Deposition efficiency (DE) is the crucial factor that indicates the productivity of the process. Based on the ISO 17836:2017 (Ref 116), DE can be calculated as

$$DE = \frac{\text{Mass difference of the test piece}}{\text{Mass of spray material fed through}} \times 100\%$$

It should be noted that usually, the calculated DE is the underestimated value because some of the feedstock material is lost in overspray and acceleration and deceleration of the torch robot. The overspray issue can be resolved (to some extent) by increasing the substrate size. The loss of material in acceleration and deceleration is

unavoidable. However, since the primary cause of the inaccuracy is the same for each session, the comparison of DEs is still valid. During suspension spray, the solvent is vaporized, only solid content reaches the substrate (for solution precursors, the estimated solid content is calculated through stoichiometric calculations) (Ref 114, 117).

Based on the DE, feedstock and other consumables cost, the coating cost of a spray process can be estimated. Here, we have assumed some spraying parameters and some are based on our previous work (Ref 118) that would help estimate the cost of TiO₂ coating deposited through SPS, SPPS and S-HVOF spray on a 1 m² substrate (Table 4).

Based on these spray parameters, the approximate cost of consumables (feedstock, power, labor, gases and water) for the coating process can be calculated for SPS, SPPS and S-HVOF, which help in estimating the coating cost (Table 5). It is worth noting that the suspension used in this cost estimation is nanoparticles (<50 nm) suspension. Usually, the cost of nanomaterials and preparation of their stable suspension is quite high and varies with the solid concentration, material, suspension medium, particle size, and place of origin. Here, we have considered a nominal range for the cost of nanomaterial suspension i.e., 200–1000 USD.

Here, we have calculated the coating cost for water as a suspension medium because despite being an energy-efficient suspension medium, ethanol (or any other alcohol) is less preferred due to the comparatively high cost and high risk of accidents. In the above scenario, for suspension, we have assumed that the solid content is homogeneously dispersed in the suspension medium. Otherwise, the requirement of external mechanical or chemical processing for homogenous dispersion increases the operational cost. For better dispersion, mechanical stirring could be a cheaper option. In the above coating cost calculation, the erosion of the plasma torch with each spray session is not considered. Here, cost estimation for only SPPS is done. In a similar way, the cost related to solution precursor HVOF spray could be calculated. Also, we have assumed that in the above example, no pretreatment (etching, grit blasting or adhesion layer) or post-treatment of the coated substrate was required.

Applications

Thermal Barrier Coatings (TBCs)

Thermal barrier coatings are constantly demanded in aviation and power generation industries to improve the efficiency and durability of turbines and engines. Typically, a thermal barrier coating system consists of two parts, i.e., dense bond coat (BC) and porous topcoat (main thermal

Table 4 Assumed spray conditions for coating deposition using SPS, SPPS and S-HVOF spray on a 1m² substrate

Parameter	SPS	SPPS	S-HVOF
Primary (Ar) and secondary (H ₂) gas flow rate (L/min ⁻¹)	50 and 0.9	50 and 0.9	...
Plasma current (A) and voltage (V)	700 and 50	700 and 50	...
Shielding gas (Ar) flow rate (L/min ⁻¹)	3	3	...
Oxygen flow rate (L/min ⁻¹)	280
Hydrogen flow rate (L/min ⁻¹)	788
Spray speed	Horizontal speed 450 mm/sec; vertical increment 5mm		
Number of passes	10	10	10
Spray time (Sec)	4444.4	4444.4	4444.4
Suspension feed rate	10 ml/min	10 ml/min	10 ml/min
Solid content (for suspension)/concentration (for solution)	5 wt.%	1M	5 wt.%
Deposition efficiency (DE)	50% (axial injection)	30% (axial injection)	50% (axial injection)

Table 5 Cost estimation of deposited coatings using SPS, SPPS and HVOF spray (based on the assumed spray parameters given in Table 4)

		Bulk Price (in USD)	Approximate cost (in USD)		
			SPS	SPPS	S-HVOF
Feedstock	Suspension (aqueous suspension of TiO ₂)	200-1000/liter	148.15-740	...	148.15-740
	TiO ₂ precursor (titanium butoxide)	118/liter	...	40.12	...
	Ethanol	55.50/liter	...	48.90	...
	Labor*	27.23 /h	...	81.69	...
Consumable	Plasma gas (Ar)	3.00/m ³	10.88	10.88	...
	Plasma gas (H ₂)	5.54/m ³	0.37	0.37	...
	Shielding gas (Ar)	3.00/m ³	0.68	0.68	...
	Oxygen	1.50/m ³	31.06
	Fuel (H ₂)	5.54/m ³	323.44
	Water for cooling	2.04/m ³	1.55	1.55	1.55
	Electricity	0.18/kWh	7.49	7.49	7.49
	Labor*	27.23/h	54.46	54.46	54.46
Total cost/m ²			223.57-815.42	164.53	579.08-1170.93

*Might vary in different parts of the world

barrier coating-TBC), where bond coat protects nickel alloy substrate against corrosion/oxidation and help topcoat adhering to the substrate. The topcoat provides thermal insulation to the substrate. The commonly used topcoat materials are zirconia and alumina-based ceramics that are widely deposited using the Electron Beam-Physical Vapor Deposition (EB-PVD) and Atmospheric Plasma Spray (APS) techniques. The high cost and low deposition rate limit the industrial application of EB-PVD. With the proof of nano-featured coatings having better strain tolerance and thermal insulation, SPS/SPPS has gained more attention

over APS. Plenty of literature suggests that the thermal resistance of TBCs could be controlled by engineering the coating microstructures such as pore size, shape, architecture and distribution. One such study found that SPS TBC exhibited ~44% and ~66% less thermal conductivity than APS and EB-PVD TBCs (Ref 119). This occurred due to the increased total porosity and nano-submicron pores in the SPS TBC, aiding better thermal insulation than micropores in APS. Besides, cauliflower-like columnar structures of SPS TBCs increase the durability of the coatings against thermal fatigue, where these columnar structures suppress

the interfacial crack propagation generated through the thermal stress (Ref 120). Similarly, ethanol-based suspensions produce TBCs with higher thermal cyclic fatigue lifetime due to the better strain tolerance of columnar microstructures than water- or water-ethanol-based suspensions (Ref 121). To tailor the thermal performance of TBCs, it is essential to understand the role of different coating parameters such as porosity, pore size distribution and columnar density (no. of columns per unit length). Recently, an understanding-based design strategy suggests that axial suspension plasma spray coatings with optimum number of pores with $>10\mu\text{m}$ and $1\mu\text{m}$ – 100nm and negligible number of pores with $10\mu\text{m}$ – $1\mu\text{m}$ and $<100\text{nm}$ should exhibit superior thermal shock performance (Ref 30). Likewise, lowering the environmental pressure during SPS can also help alter the quality of TBCs because, with the lower pressure, the columnar coating turns into a vertical crack segmented structure with the decreased roughness and increased porosity (Ref 122). According to a study, SPS TBCs are more promising than S-HVOF in producing highly porous coatings with cauliflower/column-like coating microstructures leading to lower thermal conductivity. While S-HVOF coatings are comparatively denser with vertical cracks (Ref 123).

Apart from controlling the coating microstructures, SPS and SPPS are used to customize the topcoat through doping, functionally graded or double/multi-ceramic layer designs. Although Yttria-Stabilized Zirconia (YSZ) is the well-established industrial topcoat material, to mitigate the shortcomings of YSZ such as phase transformation, thermal stability and thermal cycling life, different rare earth oxides such as Gd_2O_3 , La_2O_3 and CeO_2 are used as dopants. These dopants form nanosized clusters in the zirconia matrix, acting as defects that decrease the thermal conductivity of coating by scattering phonons (Ref 124). Developing doped coatings using APS is a complicated process as dopants power needs to be prepared through spray drying before plasma spray. In that case, liquid feedstocks are suitable to deposit dopant coatings, where YSZ particles could be suspended into precursor solution of dopants and sprayed simultaneously, or YSZ (APS) and dopant precursor solutions (SPPS) are injected sequentially. Although both approaches provide integrated advances of APS and SPPS methods, suspended particles provide high throughput and dissolved precursors give rise to nano-featured coatings with ultrafine splats, they have distinct benefits (Ref 49). The simultaneous injection gives rise to composite coatings with unique microstructures consisting of concurrently distributed nano- (due to SPPS) and micro- (due to APS) zones. The differential sintering properties of these zones hinder the densification and hence, better thermal cycling of TBC. The sequential injection develops a well-adhered layered structure with a

protective top SPPS layer that restricts the insertion of corrosive/oxidizing agent to the underlying layer and micro-porous APS layer that reduces thermal conductivity. Besides, due to the presence of the SPPS layer, the generation of thermally grown oxide (TGO), eventually slows down. According to a study, layered TBC exhibited $0.24\mu\text{m}$ thinner TGO formation after 250 thermal cycles compared to the composite TBC (Ref 49).

Apart from YSZ, zirconate with pyrochlore structures such as $\text{Gd}_2\text{Zr}_2\text{O}_7$ (GZO) or $\text{La}_2\text{Zr}_2\text{O}_7$ (LZO), are the most promising materials due to their better phase stability and low thermal conductivity. However, their low coefficient of thermal expansion (CTE) hinders their use as TBC material alone. Therefore, these materials are used in multilayered systems of functionally graded systems. The most common TBC systems are GZO/YSZ, LZO/YSZ and $\text{La}_2\text{Ce}_2\text{O}_7/\text{YSZ}$ (LCO/YSZ) systems. Despite having many advantages, layered structures might suffer from delamination during thermal cycling due to the CTE mismatch. The functionally graded coatings (FGC) could solve this problem, where different layers of YSZ and GZO or LZO with gradually varied compositions are deposited (Ref 125). In one study, where FGC of YSZ and GZO exhibited $\sim 59\%$ better resistance to thermal cycle than multilayer TBCs due to the homogenous splat formation of both coating materials, leading to uniform thermal stress and microcrack formation, and hence, the formation of longitudinal macrocracks slowed down (Ref 126). In another study, FGC-based TBC showed higher fracture toughness and better erosion resistance but inferior thermal cyclic lifetime at 1400°C than layered TBC (Ref 109). Some examples of different thermal barrier coatings deposited using liquid-based thermal spray methods are summarized in Table 6. Even though these ways of modifying the coating microstructures and architecture using liquid feedstocks provide the versatility to deposit next-generation TBC coatings, the feasibility of applying these coatings, replacing the conventional APS remains challenging. Hence, the development and optimization of these multi-layer models need to be done.

Erosion- and Wear-Resistant Coatings

Stability against wear, abrasion and erosion are other desired properties for thermal barrier coatings. Usually, electron beam-physical vapor deposition (EB-PVD)-based coatings exhibit better erosion and wear resistance than APS coatings due to their columnar architecture. But their high production cost hinders their commercial application. Suspension or solution precursor-based plasma/HVOF coatings, possessing nano- and submicron sized splats, unique morphologies including columnar/vertically cracked coating microstructures, exhibiting better strain-

Table 6 Examples of different thermal barrier coatings deposited using liquid feedstock for thermal spray

TBC material	Bond coat material	Substrate	Spray method	Thermal conductivity (W/(m.K))	Thermal cyclic fatigue lifetime	Reference
8YSZ	NiCoCrAlY	Hastelloy®X	SPS	0.85 to 1 (for ethanol-based suspensions) 0.83 (for water-based suspensions) 1.3 (for water + ethanol-based suspensions)	380–480 cycles (1h at 1100 °C)	(Ref 121)
8YSZ-SiO ₂	8YSZ	Al-Si alloy	SPS	0.389 (as sprayed) to 0.261 (after thermal shock for 1 s at 800 °C)	...	(Ref 127)
8YSZ	NiCoCrAlY	Hastelloy®X	SPS SHVOF	For SPS: 0.56-0.9 (as sprayed) & 1.8-1.3 (after thermal treatment*) For S-HVOF: 0.86-1.29 (as sprayed) & 1.13-2.09 (after thermal treatment*) (* thermal treatment conditions: room temperature to 1190 °C in 4h)	For SPS <3um: 263 ± 86 cycles For SPS <10um: 323 ± 15 cycles For S-HVOF <3um: 226 ± 78 cycles For S-HVOF<10um: 230 ± 38 (test conditions: 1100 °C for a period of 1 h)	(Ref 123)
Strontium zirconate (SrZrO ₃)	...	Graphite	SPPS	~1.25 (as sprayed; at 1000 °C)	...	(Ref 128)
YAG (yttrium aluminum garnet)	MCrAlY	304 stainless steel	SPPS	1.68 (at room temperature) to 0.91 (at 1300 °C)	~1200 cycles (at 1121 °C for 1h), ~600 cycles (at 1150 °C for 1h) and ~1400 cycles (at 1150° C for 8h)	(Ref 129)
L ₂ Ce ₂ O ₇ (LCO)	NiCoCrAlY	Superalloy	SPPS	0.50-0.75 (as sprayed; at 1200 °C)	...	(Ref 130)
Gadolinium Zirconate, Gd ₂ Zr ₂ O ₇ (GZO)	NiCrAlY	OEM superalloy	SPPS	...	206 cycles (1180 °C for 1 h)	(Ref 131)

tolerant behavior, that make them a suitable choice for erosion and wear resistant applications (Ref 28, 129, 132). Apart from the spray method, other factors such as porosity content, hardness and toughness of the coating influence the erosion and wear behavior of a coating (Ref 129, 133). Higher porosity leads to an easy removal/detachment of the coating material from the coating matrix. To resolve this issue, an additional dense layer is deposited on the top that improves erosion resistance (Ref 133). Some examples of different erosion resistant coatings deposited using liquid-based thermal spray methods are summarized in Table 7.

Corrosion-Resistant Coatings

Corrosion is an inevitable threat to various industries, leading to the deterioration and failure of the component/system. Usually, coatings (passive or active) are used to protect the surface and delay corrosion. Due to their robust nature, thermal spray coatings are constantly being used for various applications such as orthopedics, turbines, offshore structures and engines to protect the surface against corruptions. It is proven that the corrosion stability varies with coating microstructures. For instance, SPS hydroxyapatite (HAp) coatings showed better corrosion resistance in fetal bovine serum (FBS) than APS HAp coatings (Ref 136). The reason was that the lamellar microstructures with micro-size cracks in APS HAp coatings acted like micro-capillaries, helping FBS reach the substrate and lead to corrosion. Since the coating development method affects the corrosion performance of the coating material, suspension and solution precursor-based coatings vary in their corrosion performances. SPS HAp coatings were found to be more stable in Hank's medium than the SPPS HAp coatings attributed to the well-melted splats, giving rise to

a comparatively denser coating structure (Ref 137). While for SPPS HAp coating, various large-size pores with partially melted/unmelted particles along with some fully melted particles were observed.

Suspension and solution precursor-based HVOF or plasma spray coatings also help control another type of corrosion, i.e., hot corrosion. It is prevalent in TBCs when molten deposits from impurities in the fuel such as sodium, sulfur, vanadium, lead, and phosphorus settle on coatings. During combustion, these impurities oxidize and form a strong acidic or alkaline molten oxide, deteriorating the ceramic and metallic parts of the TBC system through selective leaching of the stabilizer from zirconia, resulting in phase change and consequently volume changes $\sim 3\text{--}5\%$ upon cooling (Ref 138). The corrosion resistance of thermal spray coatings could be improved either by altering the coating architecture or incorporating certain oxygen-active elements into the coating. Usually, higher porosity is preferred in TBCs due to better strain tolerance and lower thermal conductivity, but it is not beneficial for erosion and hot corrosion resistance because of infiltration of molten salts and other impurities into the TBC system (Ref 138). Suspension and solution precursor plasma and HVOF spray provide the freedom to control pores and splats boundaries. It was found that a mixed (suspension + solution precursor based) YSZ coating exhibited slightly better hot corrosion resistance than a conventional (APS) YSZ coating due to smaller grain size (20–30nm) and pores (Ref 139). After a four-hour hot corrosion test, the mixed YSZ coating did not show severe degradation (some vertical or oblique cracks in the coating), while for APS-YSZ coating, degradation took place at ceramic–bond coat interface (large transverse cracks). Another way to improve the corrosion resistance is to design TBCs with a less reactive topcoat material or a

Table 7 Examples of erosion resistant coatings deposited using liquid feedstock-based plasma/HVOF spray methods

Coating material	Coating method	Porosity	Microhardness	Erosion rate/erosivity number/ erosion wear rate	Reference
Yttrium aluminum garnet (YAG; $\text{Y}_3\text{Al}_5\text{O}_{12}$)	SPPS	30.5 ± 2.5 vol.%	258 ± 28	*0.18–0.23 (g/kg)	(Ref 129)
$\text{Al}_2\text{O}_3\text{-YSZ/ZrO}_2$	Hybrid powder+ S-HVOF	...	823–1032 @ $\text{HV}_{0.3}$...	(Ref 47)
Gadolinium zirconate/YSZ (GZ/YSZ)	SPS (composite & layered architecture)	16–18 vol.%	...	#1.9–2.2 seconds/mils	(Ref 109)
GZ/YSZ	SPS GZ-dense/GZ/YSZ	~ 15 vol.%	646 ± 35 @ $\text{HV}_{0.5}$	# ~ 3 seconds/mils	(Ref 133)
YAG	SPPS	33–44 vol.%	...	*0.23–2.81 (g/kg)	(Ref 134)
$\text{Al}_2\text{O}_3\text{-YSZ}$	Hybrid powder + SPS	3.3 ± 0.5 area%	1096 ± 136 @ $\text{HV}_{0.1}$	\$ $\sim 0.06\text{--}0.1 \times 10^{-3}$ g/gm	(Ref 135)

*= Erosion rate; # = Erosivity number; \$ = Erosion wear rate

dense sealing layer. Satyapal et al. (Ref 138) found that between layered (GZ dense/GZ/YSZ) and composite (GZ + YSZ/YSZ) TBCs, layered TBC exhibited inferior hot corrosion-induced fracture toughness, resulting in a larger number of horizontal cracks near the interface attributing to the absence of the dense sealing layer at the columnar region. While composite TBC restricted the molten salt after reacting with it in the top composite layer (GZ+YSZ), and hence, showed horizontal cracks close to the top surface instead on interfacial region.

Electronic Applications

Most thermal spray studies focus on protective coatings rather than functional such as dielectric, conductive, luminescent and bioactive coatings. The development of a fundamental understanding of the process and process-materials-property relationship opens an innovative path of opportunities in the fields of electronics, ceramic superconductors and sensors. For instance, liquid feedstock-based plasma and HVOF spray could be used to develop reflective coatings suitable for a large range of wavelengths due to having pores acting as several optical index discontinuities, exhibiting high reflectivity. Marthe et al. (Ref 140) developed a self-supported bi-layer coating of alumina, with >90% scattered reflectance for UV–visible range of wavelengths. The first layer (micro-structured layer) was developed using APS that with ~200nm average pore size efficiently scattered only at the longer wavelengths (500-800nm) radiation, and the second layer that was developed using SPS scattered the radiation at the lowest wavelengths (300-500 nm) only due to having smaller pores (<80 nm). The scattering property of both coatings did not interfere with each other as for APS coating, and the pores were too big to scatter the shorter wavelength radiation and similarly, for SPS coating, the pores were too small to scatter longer wavelength radiation. Similarly, the electrical properties of a coating vary with the shape and the distribution of the microstructural defects, i.e., pores and cracks (Ref 141). For example, yttrium oxide coatings deposited using SPS exhibit higher dielectric breakdown voltage due to having higher coating density and lower surface roughness, leading to reduced electrical stresses and measurement errors occurring at the coating and electrode interfaces than the APS yttrium coatings (Ref 141). In a study, S-HVOF alumina coatings exhibited better electrical resistivity and stability at very high humidity (97% RH) than the conventional HVOF coatings (Ref 142). Conventional HVOF coatings, having interconnected cracks and pores that helped in adsorption and accumulation of water monolayers on the oxide surface, showed increased surface electrical conductivity. Contrastingly, the dielectric strength of S-HVOF alumina

coating was slightly inferior to the conventional HVOF coatings because the micro-scale defects (pores or cracks) in S-HVOF were significant enough to induce the formation and concentration of high electrical field densities. However, since these micro-defects were homogeneously distributed in the coating matrix, the fluctuation in dielectric strength with changing coating thickness was lower than conventional HVOF coatings.

Plasma and HVOF spray are also used to deposit perovskite materials that are widely employed in solid oxide fuel cells (SOFC). Since these ceramics often have complex compositions, the inhomogeneous dissociation and evaporation behavior of individual constituents change the chemical composition and lead to the formation of secondary phases in the coating matrix that ultimately affects the coating performance as a cathode, anodes or electrolytes (Ref 143). The purity of perovskite materials could be enhanced by further treating them at high temperatures in a furnace in the presence of oxygen, which is energy and time-consuming. By optimizing the spray parameters using suspension or solution-based plasma spray and HVOF, a wide variety of coating structures with different compositions without further post-deposition sintering requirements could be produced (Ref 143-145). Likewise, the liquid feedstock-based plasma or HVOF spray provides better control over the electrochemical performance of the solid electrolyte (Ref 146, 147). For instance, for lower energy plasma spray, flammable (ethanol and/or ethylene glycol) suspension medium exhibits better YSZ electrolyte conductivity in SOFC than a water-based suspension medium YSZ electrolyte (Ref 145). Also, it was found that the electrolyte conductivity was the same for suspension and solution precursor YSZ electrolytes, but the latter showed more gas leakage rate than the suspension electrolyte. During operation, SOFCs generally suffer from chromium poisoning that affects the cathode performance negatively and increases interfacial resistance, and to resolve this issue, a conductive protective coating on current collectors and interconnectors is required (Ref 148). Spinel metal oxide coatings are considered a promising solution to this issue due to having better electrical conductivity and chemical and structural stability at elevated temperatures, but thick film deposition of these oxides (especially on current collector mesh) using a cost-efficient method is another issue. SPPS, being a versatile technique, provides better control over the coating stoichiometry, thickness and morphology. It was found that SPPS deposited manganese cobalt oxide ($Mn_{1.5}Co_{1.5}O_4$) coatings on mesh and plates in SOFC provide good oxidation resistance and low area-specific resistance, which was stable for more than 72 hours (Ref 149).

Suspension and solution precursor-based plasma and HVOF spray coatings are also used for sensing

applications. Conventional techniques to alter a bandgap of semiconductor metal oxides through doping are tedious and require expensive facilities. Self-doping with oxygen vacancies provides an alternative approach to narrow the bandgap (Ref 150), and with an increased number of oxygen vacancies, visible light responding could be achieved. As the size of the oxide semiconductor decreases, the oxygen vacancy content also increases. Using the SPPS process combines the nanomaterial synthesis with high-temperature heating and rapid cooling in reducing atmosphere that helps in generating a large number of oxygen vacancies in wide bandgap semiconductor coatings (Ref 151–153). Besides, the large surface area and porous structure of SPPS coatings help in improving the sensitivity of the sensor (Ref 153, 154). Apart from that, using different starting solution precursors, the coating microstructures and their sensitivity toward different molecules could be varied (Ref 155). Also, with SOD increments, the response time and recovery time of ZnO coating toward sensing NO_2 decrease due to the increased porosity, and SOD 100mm showed the best sensing response (Ref 152). Solution precursor-based spray is proven an excellent method to enhance the sensing performance of composite coatings due to donor defects and homogenous heterojunctions (Ref 154). So, selecting the deposition parameters carefully, functional and smart coatings could be developed.

Other Smart Coatings

Self-healing coatings are in demand in multiple areas due to their ability to repair cracks and defects within coatings without any external intervention, extending their service time. TBCs that ultimately undergo coating spallation due to the thermos-mechanical loading, which develop cracks in the coating, could be resolved by incorporating some healing agents such as SiC, MoSi_2 , and TiC, that after exposing to a high-temperature atmosphere, forms oxides and heal the pores or cracks in the coatings (Ref 156–158). It is essential to avoid undesired reactions and premature oxidation of the healing agent during the coating deposition. Suspension and solution-based feedstocks are very suitable for plasma spray because a part of the plasma energy becomes utilized in solvent evaporation, shielding the material against early oxidation (Ref 159). But simultaneously, sufficient energy should be transferred to the solid material for proper melting and adhering to the substrate after hitting it. Otherwise, poor intersplat interactions would give rise to poor mechanical and thermal properties of the coating (Ref 25). Hence, the understanding and optimization of deposition parameters and feedstock properties are essential. Sol-gel glassification could be a solution to this situation, where the healing agent is

encapsulated by a stable ceramic layer like Al_2O_3 or SiO_2 , providing better thermal durability to the coating (Ref 157, 160). The poor fluidity of the healing agents restricts their potential use to fill the larger cracks, which could be overcome by doping appropriate material, optimizing encapsulation and feedstock properties.

Thermal spray coatings often show superhydrophobicity. Superhydrophobic surfaces i.e., surfaces that exhibit water contact angle (WCA) $>150^\circ$ and roll-off angles (RA) $<10^\circ$ show water-repellency and provide various additional functions such as self-cleaning, corrosion protection and anti-biofouling. The surface wettability generally depends on the surface chemical composition and surface topography, and the use of liquid feedstock in plasma and HVOF spraying gives the freedom of controlling both properties (Ref 161). Although a wide range of approaches is used to develop superhydrophobic coatings/surfaces, low time- and cost-efficiency and poor durability of coatings developed using these methods restrict their large-scale fabrication. Due to the use/formation of nanomaterials during spray, liquid feedstock-based plasma and HVOF coatings show multi-scale roughness, mimicking the surface of some superhydrophobic leaves in nature (Ref 162). In a study, coatings deposited using different SODs (30, 40 and 50mm) showed WCA $>150^\circ$. However, due to the varied coating microstructures, the WCA and RA values were different (Ref 163). The coatings deposited at 30 mm SOD showed $\sim 163^\circ$ WCA and $\sim 6.4^\circ$ RA due to having dense and close-patterned columnar structures with high aspect ratio in the coating, which trapped the air between deep crevices more efficiently than the coatings deposited at 40 and 50 mm. With increased SOD, the intercolumnar gap became broader and shallower, allowing water droplet penetration and reduced WCA. It was observed that coatings deposited using a smaller number of passes (15) showed better superhydrophobicity (WCA $\sim 155^\circ$) than the coatings deposited using more number of passes (25 passes with WCA 140°) (Ref 162). The reason behind this is the formation of feathery features at an increased number of passes due to the shadowing effect that aids in water penetration and reducing the contact angle (CA). Although adding a layer of a low-surface-energy polymer on the thermal spray coatings also introduces superhydrophobicity to the coatings surface, the durability of the polymeric layer against the harsh environmental condition is an issue.

Liquid feedstock-based plasma spray, especially SPPS, has the potential to develop robust superhydrophobic coatings and could be used to develop surfaces with reversible wettability. Xu et al. (Ref 164) deposited Yb_2O_3 coatings with a WCA $\sim 160^\circ$ and RA $\sim 7^\circ$ using low-pressure SPPS. They demonstrated that after prolonged exposure (at 200°C for 5h) of thermal annealing, the coating lost its water-repellency and turned into

superhydrophilic coatings. The superhydrophobicity could be regained after vacuum treatment of the coating, representing its reversible wettability feature. Some of the examples of superhydrophobic coatings deposited using the liquid feedstock-based thermal spray method are summarized in Table 8. Solution precursor-based spray provides better control over the coating chemistry and microstructures is a potential tool to develop superhydrophobic coatings, but limited information about parameters-property correlation and low deposition efficiency hinders its potential applications.

Another application of liquid feedstock plasma and HVOF spray is antimicrobial coatings for various surfaces, including implants, where suspension and solution precursor help doping the hydroxyapatite coatings with antimicrobial materials like silver, zinc, copper, etc. (Ref 171, 172). Some of the examples of antimicrobial coatings deposited using liquid feedstock in the thermal spray are presented in Table 9. The elimination of tedious powder preparation methods and homogenous distribution of the doping material are the two main benefits of using liquid feedstocks (Ref 173). Even though suspension and solution precursor plasma and HVOF spray open the door of opportunities to develop novel coatings with desired structures and properties by controlling the deposition parameters and feedstock properties, more research focused on the parameters-property relationship is required.

Outlook

Suspension and solution precursor plasma and HVOF spray offer the benefits of developing a wide range of coatings with unique microstructures such as columnar or vertically segmented. In the past few years, with technological advancements such as development of suitable guns, injectors, diagnostic tools, etc., the liquid feedstock-based plasma and HVOF spray have become capable of meeting the manufacturing standards as well as end user requirements. Suspension and solution precursor-based coatings are already being used in various industries for different applications.

Due to the complexity of the process, there are some challenges that need to be overcome for further improvement of the process. For example, liquid feedstock-based thermal spray has low throughput than powder feedstock-based thermal spray, but the optimized suspension and solution precursor feedstock have the capability to surpass the deposition efficiency of APS. Although complex feedstock preparation and their high cost is the foremost concern but with technical advancements, this could be improved. Further, technological readiness of these

Table 8 Examples of superhydrophobic coatings deposited using liquid feedstock-based plasma/HVOF spray methods

Coating material	Spray method	Substrate	Water contact angle	Roll-off angle	Sliding angle	Reference
Yb ₂ O ₃	SPPS	304 stainless steel	163 ± 1.5°	6.5°	...	(Ref 165)
ZnO	SPPS	Wood surface	120° ± 4°	(Ref 166)
CeO ₂	S-HVOF	Aluminum alloy (1050A), stainless steel (AISI 304)	130-140°	(Ref 167)
TiO ₂	SPS	Nickel Alloy (NIMONIC C263), stainless steel	~ 167°	...	~ 1.3°	(Ref 161)
ZnO	SPPS	Aluminum plates	136°	(Ref 168)
Yb ₂ O ₃	Solution precursor vacuum plasma spray	304 stainless steel	At 30mm: 163° At 80mm: 141° At 90mm: 140° At 100mm: 138°	At 30mm: ~6°	...	(Ref 169)
TiO ₂ /h-BN	S-HVOF	304 stainless steel	163-170°	15 to 30°	...	(Ref 170)

Table 9 Examples of antimicrobial coatings deposited using liquid feedstock-based plasma/HVOF spray methods

Coating material	Substrate	Spray method	Microorganisms	Reference
Zn-doped HAp	Ti-6Al-4V	SPFS	Escherichia coli and Staphylococcus aureus	(Ref 174)
Soda-lime glass	Titanium grade 2 plates	SHVOF	Escherichia coli, Staphylococcus aureus and Candida krusei	(Ref 175)
TiO ₂ -HA-rGO nanocomposite	316L stainless steel plates	Suspension flame spray	Escherichia coli	(Ref 176)
TiO ₂ -SrCO ₃ composite	316L stainless steel	SPS	Escherichia coli	(Ref 177)
Fluoridated hydroxyapatite (FHA)	Titanium grade 2 plates	SPS	Staphylococcus aureus	(Ref 178)

techniques could be improved by understanding feedstock and energy source/gas interactions along with coating formation mechanism through experimental analyses and numerical simulations. Also, the development of new sensors for the velocity and temperature measurement of sprayed particles will help provide better control over the process. Another way of improvement in liquid feedstock-based coating deposition is developing coatings using hybrid feedstock/injection that introduces unique features into the coating, but for their potential application, more work is required to optimize the spray parameters in a way that they are suitable for both powder as well as suspension/solution, making the process robust and reliable for industrial adoption.

In short, coatings generated through liquid feedstock-based plasma/HVOF spray are more beneficial than conventional coatings but to exploit their full potential further efforts are required.

Acknowledgements This project has received funding from the European Union's Horizon 2020 research and innovation programme under the project: GeoHex-advanced material for cost-efficient and enhanced heat exchange performance for geothermal application (Grant agreement 851917). We want to acknowledge the contribution of the GeoHex consortium in this project.

Open Access This article is licensed under a Creative Commons Attribution 4.0 International License, which permits use, sharing, adaptation, distribution and reproduction in any medium or format, as long as you give appropriate credit to the original author(s) and the source, provide a link to the Creative Commons licence, and indicate if changes were made. The images or other third party material in this article are included in the article's Creative Commons licence, unless indicated otherwise in a credit line to the material. If material is not included in the article's Creative Commons licence and your intended use is not permitted by statutory regulation or exceeds the permitted use, you will need to obtain permission directly from the copyright holder. To view a copy of this licence, visit <http://creativecommons.org/licenses/by/4.0/>.

References

1. E. Dongmo et al., Modeling of Combustion as well as Heat, Mass, and Momentum Transfer During Thermal Spraying by HVOF and HVFS, *J. Therm. Spray Technol.*, 2009, **18**(5), p 896.
2. S. Joshi and P. Nylen, Advanced Coatings by Thermal Spray Processes. *Technologies*, 2019, **7**(4), p 79.
3. P. Fauchais et al., What Do We Know, What are the Current Limitations of Suspension Plasma Spraying?, *J. Therm. Spray Technol.*, 2015, **24**(7), p 1120–1129.
4. D. Tejero-Martin et al., Beyond Traditional Coatings: A Review on Thermal-Sprayed Functional and Smart Coatings, *J. Therm. Spray Technol.*, 2019, **28**(4), p 598–644.
5. Y. Zhao et al., Parametric Analysis and Modeling for the Porosity Prediction in Suspension Plasma-Sprayed Coatings, *J. Therm. Spray Technol.*, 2020, **29**(1), p 51–59.
6. X. Chen et al., Effects of Processing Parameters on the Deposition of Yttria Partially Stabilized Zirconia Coating During

- Suspension Plasma Spray, *J. Am. Ceram. Soc.*, 2016, **99**(11), p 3546–3555.
7. X. Meng et al., Thermal Decomposition and Crystallization Behavior of Double Rare-Earth Co-Doped SrZrO₃ Precursor Used in the Solution Precursor Plasma Spray Process, *Surf. Coat. Technol.*, 2019, **369**, p 87–94.
 8. L. Pawlowski, Suspension and Solution Thermal Spray Coatings, *Surf. Coat. Technol.*, 2009, **203**(19), p 2807–2829.
 9. A. Killinger, P. Müller and R. Gadow, What Do We Know, What are the Current Limitations of Suspension HVOF Spraying?, *J. Therm. Spray Technol.*, 2015, **24**(7), p 1130–1142.
 10. N. Markocsan et al., Liquid Feedstock Plasma Spraying: An Emerging Process for Advanced Thermal Barrier Coatings, *J. Therm. Spray Technol.*, 2017, **26**(6), p 1104–1114.
 11. G. Mauer and R. Vaßen, Coatings with Columnar Microstructures for Thermal Barrier Applications, *Adv. Eng. Mater.*, 2020, **22**(6), p 1900988.
 12. P. Fauchais et al., Key Challenges and Opportunities in Suspension and Solution Plasma Spraying, *Plasma Chem. Plasma Process.*, 2015, **35**(3), p 511–525.
 13. J. Kiilakoski et al., Process Parameter Impact on Suspension-HVOF-Sprayed Cr₂O₃ Coatings, *J. Therm. Spray Technol.*, 2019, **28**(8), p 1933–1944.
 14. Y. Zhao et al., Evaluation of Nano/Submicro Pores in Suspension Plasma Sprayed YSZ Coatings, *Surf. Coat. Technol.*, 2019, **378**, p 125001.
 15. S. Khan et al., Structural and Hydrophilic Properties of TiN Films Prepared by Ultrasonic Atomization Assisted Spray Method Under Low Temperature, *Surf. Coat. Technol.*, 2020, **393**, p 125824.
 16. K. VanEvery et al., Column Formation in Suspension Plasma-Sprayed Coatings and Resultant Thermal Properties, *J. Therm. Spray Technol.*, 2011, **20**(4), p 817–828.
 17. M. Chambard et al., Effect of the Deposition Route on the Microstructure of Plasma-Sprayed Hydroxyapatite Coatings, *Surf. Coat. Technol.*, 2019, **371**, p 68–77.
 18. A. Förg et al., Suspension and Coating Characterization of High Velocity Suspension Flame Sprayed (HVFSF) Mixed Titanium Oxide–Titanium Carbide Coatings, *Surf. Coat. Technol.*, 2019, **371**, p 90–96.
 19. E. Gozali, S. Kamnis and S. Gu, Numerical Investigation of Combustion and Liquid Feedstock in High Velocity Suspension Flame Spraying Process, *Surf. Coat. Technol.*, 2013, **228**, p 176–186.
 20. S. Gu and S. Kamnis, Numerical Modelling of In-Flight Particle Dynamics of Non-Spherical Powder, *Surf. Coat. Technol.*, 2009, **203**(22), p 3485–3490.
 21. K. Zhang, H.-B. Xiong and X.-M. Shao, Dynamic Modeling of Micro- and Nano-Sized Particles Impinging on the Substrate During Suspension Plasma Spraying, *J. Zhejiang Univ. Sci. A*, 2016, **17**(9), p 733–744.
 22. A. Ganvir et al., Experimental Visualization of Microstructure Evolution During Suspension Plasma Spraying of Thermal Barrier Coatings, *J. Eur. Ceram. Soc.*, 2019, **39**(2), p 470–481.
 23. J.-K. Lee et al., Fragmentation Behavior of Y₂O₃ Suspension in Axially Fed Suspension Plasma Spray, *Surf. Coat. Technol.*, 2017, **309**, p 456–461.
 24. F. Tarasi et al., Effective Parameters in Axial Injection Suspension Plasma Spray Process of Alumina–Zirconia Ceramics, *J. Therm. Spray Technol.*, 2008, **17**(5), p 685–691.
 25. V. Carnicer et al., Aqueous Suspension Processing of Multi-component Submicronic Y-TZP/Al₂O₃/SiC Particles for Suspension Plasma Spraying, *J. Eur. Ceram. Soc.*, 2018, **38**(5), p 2430–2439.
 26. V. Carnicer et al., Influence of Solids Concentration on the Microstructure of Suspension Plasma Sprayed Y-TZP/Al₂O₃/SiC Composite Coatings, *Surf. Coat. Technol.*, 2019, **371**, p 143–150.
 27. N. Curry et al., Performance Testing of Suspension Plasma Sprayed Thermal Barrier Coatings Produced with Varied Suspension Parameters, *Coatings*, 2015, **5**(3), p 338–356.
 28. M. Michalak et al., Wear Behavior Analysis of Al₂O₃ Coatings Manufactured by APS and HVOF Spraying Processes Using Powder and Suspension Feedstocks, *Coatings*, 2021, **11**(8), p 879.
 29. A. Ganvir et al., Deposition of Hydroxyapatite Coatings by Axial Plasma Spraying: Influence of Feedstock Characteristics on Coating Microstructure, Phase Content and Mechanical Properties, *J. Eur. Ceram. Soc.*, 2021, **41**(8), p 4637–4649.
 30. A. Ganvir et al., Tailoring Columnar Microstructure of Axial Suspension Plasma Sprayed TBCs for Superior Thermal Shock Performance, *Mater. Des.*, 2018, **144**, p 192–208.
 31. F. Venturi, J. Pulsford and T. Hussain, A Novel Approach to Incorporate Graphene Nanoplatelets to Cr₂O₃ for Low-Wear Coatings, *Mater. Lett.*, 2020, **276**, p 128283.
 32. M. Michalak et al., A Study on the Microstructural Characterization and Phase Compositions of Thermally Sprayed Al₂O₃-TiO₂ Coatings Obtained from Powders and Water-Based Suspensions, *Materials*, 2020, **13**(11), p 2638.
 33. P. Puddu et al., Suspension HVOF Spraying of TiO₂ Using a Liquid-Fueled Torch, *Surf. Coat. Technol.*, 2018, **349**, p 677–694.
 34. R. Rampon et al., Influence of Suspension Characteristics on Coatings Microstructure Obtained by Suspension Plasma Spraying, *Surf. Coat. Technol.*, 2008, **202**(18), p 4337–4342.
 35. F. Tarasi et al., A Comparative Study of YSZ Suspensions and Coatings, *Coatings*, 2019, **9**(3), p 188.
 36. M. Jadidi et al., Heat Transfer in Suspension Plasma Spraying, *Handbook of Thermal Science and Engineering*. Springer International Publishing, Cham, 2018, p 2923–2966
 37. M. Taleby and S. Hossainpour, Numerical Investigation of High Velocity Suspension Flame Spraying, *J. Therm. Spray Technol.*, 2012, **21**(6), p 1163–1172.
 38. M. Blum et al., High Velocity Suspension Flame Spraying (HVFSF) of Metal Suspensions, *Materials (Basel, Switzerland)*, 2020, **13**(3), p 621.
 39. P. Sokołowski et al., The Microstructural Studies of Suspension Plasma Sprayed Zirconia Coatings with the Use of High-Energy Plasma Torches, *Surf. Coat. Technol.*, 2017, **318**, p 250–261.
 40. H. Hou et al., Hybrid Suspension/Solution Precursor Plasma Spraying of a Complex Ba(Mg_{1/3}Ta_{2/3})O₃ Perovskite: Effects of Processing Parameters and Precursor Chemistry on Phase Formation and Decomposition, *J. Therm. Spray Technol.*, 2019, **28**(1), p 12–26.
 41. G. Sivakumar et al., Effect of SPPS Process Parameters on In-Flight Particle Generation and Splat Formation to Achieve Pure α -Al₂O₃ Coatings, *J. Therm. Spray Technol.*, 2015, **24**(7), p 1221–1234.
 42. C.K. Muoto et al., Identification of Desirable Precursor Properties for Solution Precursor Plasma Spray, *J. Therm. Spray Technol.*, 2011, **20**(4), p 802.
 43. S. Björklund, S. Goel and S. Joshi, Function-Dependent Coating Architectures by Hybrid Powder-Suspension Plasma Spraying: Injector Design, Processing and Concept Validation, *Mater. Des.*, 2018, **142**, p 56–65.
 44. S.V. Joshi and G. Sivakumar, Hybrid Processing with Powders and Solutions: A Novel Approach to Deposit Composite Coatings, *J. Therm. Spray Technol.*, 2015, **24**(7), p 1166–1186.
 45. K. Chen et al., Loading of Zn/ZnO Particles in the Precursor Feedstock Affects the Characteristics of Liquid Plasma Sprayed Nano-ZnO Coatings for Photocatalytic Applications, *Nanotechnology*, 2020, **31**(18), p 185301.

46. W.-W. Zhang et al., Bimodal TBCs with Low Thermal Conductivity Deposited by a Powder-Suspension Co-Spray Process, *J. Mater. Sci. Technol.*, 2018, **34**(8), p 1293–1304.
47. J. Kiilakoski et al., Characterization of Powder-Precursor HVOF-Sprayed Al₂O₃-YSZ/ZrO₂ Coatings, *J. Therm. Spray Technol.*, 2019, **28**(1), p 98–107.
48. A. Lohia et al., Deposition of Nanocomposite Coatings Employing a Hybrid APS + SPPS Technique, *J. Therm. Spray Technol.*, 2014, **23**(7), p 1054–1064.
49. S.V. Joshi et al., Hybrid Plasma-Sprayed Thermal Barrier Coatings Using Powder and Solution Precursor Feedstock, *J. Therm. Spray Technol.*, 2014, **23**(4), p 616–624.
50. F.S. Miranda et al., High-Velocity Plasma Spray Process Using Hybrid SiO₂ + ZrO₂ Precursor for Deposition of Environmental Barrier Coatings, *Surf. Coat. Technol.*, 2020, **404**, p 126447.
51. S. Mahade et al., Novel Wear Resistant Carbide-Laden Coatings Deposited by Powder-Suspension Hybrid Plasma Spray: Characterization and Testing, *Surf. Coat. Technol.*, 2020, **399**, p 126147.
52. S. Mahade et al., Novel Utilization of Powder-Suspension Hybrid Feedstock in HVOF Spraying to Deposit Improved Wear and Corrosion Resistant Coatings, *Surf. Coat. Technol.*, 2021, **412**, p 127015.
53. J. Oberste-Berghaus, S. Bouaricha, J.-G. Legoux, C. Moreau, B. Harvey, *Method and apparatus for fine particle liquid suspension feed for thermal spray system and coatings formed therefrom*, in US8629371B2, N.R.C.o. Canada, Editor. (2005)
54. P. Carpio et al., Solution Concentration Effect on Mechanical Injection and Deposition of YSZ Coatings Using the Solution Precursor Plasma Spraying, *Surf. Coat. Technol.*, 2019, **371**, p 124–130.
55. P. Fauchais et al., Parameters Controlling Liquid Plasma Spraying: Solutions, Sols, or Suspensions, *J. Therm. Spray Technol.*, 2008, **17**(1), p 31–59.
56. H.-B. Xiong et al., Effects of Atomization Injection on Nanoparticle Processing in Suspension Plasma Spray. *Nanomaterials*, 2016, **6**(5), p 94.
57. M. Gell et al., Thermal Barrier Coatings Made by the Solution Precursor Plasma Spray Process, *J. Therm. Spray Technol.*, 2008, **17**(1), p 124–135.
58. E.H. Jordan, M.G., P. Bonzani, D. Chen, S. Basu, B. Cetegen, F. Wu, and X. Ma. *Making Dense Coatings with the Solution Precursor Plasma Spray Process*. in *Thermal Spray 2007: Global Coating Solutions*. 2007. Materials Park, OH, USA: ASM International
59. O. Marchand et al., An Insight into Suspension Plasma Spray: Injection of the Suspension and Its Interaction with the Plasma Flow, *J. Therm. Spray Technol.*, 2011, **20**(6), p 1310–1320.
60. T. Tesar et al., Development of Suspension Plasma Sprayed Alumina Coatings with High Enthalpy Plasma Torch, *Surf. Coat. Technol.*, 2017, **325**, p 277–288.
61. M. Mahrukh, A. Kumar and S. Gu, Effects of Angular Injection, and Effervescent Atomization on High-Velocity Suspension Flame Spray Process, *Surf. Coat. Technol.*, 2016, **302**, p 368–382.
62. S.A. Esfarjani and A. Dolatabadi, A 3D Simulation of Two-Phase Flow in an Effervescent Atomizer for Suspension Plasma Spray, *Surf. Coat. Technol.*, 2009, **203**(15), p 2074–2080.
63. W. Ma et al., Deposition Characteristics of SrZrO₃ Thermal Barrier Coating Prepared by Solution Precursor Plasma Spray Process, *J. Therm. Spray Technol.*, 2019, **28**(1), p 189–197.
64. M. Aghasibeig et al., A Review on Suspension Thermal Spray Patented Technology Evolution, *J. Therm. Spray Technol.*, 2019, **28**(7), p 1579–1605.
65. E.M. Cotler, D. Chen and R.J. Molz, Pressure-Based Liquid Feed System for Suspension Plasma Spray Coatings, *J. Therm. Spray Technol.*, 2011, **20**(4), p 967–973.
66. Z.C. Alexander Korolev, *Injector for plasma spray torches*, in US20130098880A1, N.M. Corp, Editor. (2011)
67. W.F. Werkheiser, B.T. Hazel, J.F. Blondin, *Suspension plasma spray apparatus and use methods*, in US9669365B2, R.T. Corp, Editor. (2014)
68. F.-L. Toma et al., Demands, Potentials, and Economic Aspects of Thermal Spraying with Suspensions: A Critical Review, *J. Therm. Spray Technol.*, 2015, **24**(7), p 1143–1152.
69. A. Potthoff et al., Development and Application of Binary Suspensions in the Ternary System Cr₂O₃-TiO₂-Al₂O₃ for S-HVOF Spraying, *J. Therm. Spray Technol.*, 2018, **27**(4), p 710–717.
70. F. Venturi and T. Hussain, Radial Injection in Suspension High Velocity Oxy-Fuel (S-HVOF) Thermal Spray of Graphene Nanoplatelets for Tribology, *J. Therm. Spray Technol.*, 2020, **29**(1), p 255–269.
71. F. Jabbari et al., A Numerical Study of Suspension Injection in Plasma-Spraying Process, *J. Therm. Spray Technol.*, 2014, **23**(1), p 3–13.
72. S. Chadha et al., A Computational and Experimental Investigation into Radial Injection for Suspension High Velocity Oxy-Fuel (SHVOF) Thermal Spray, *J. Therm. Spray Technol.*, 2019, **28**(6), p 1126–1145.
73. B. T. Hazel, X. Liu, *Suspension plasma spray apparatus and use methods*, in EP3192891A1, R.T. Corp, Editor. (2016)
74. E. Dongmo et al., Numerical Approach and Optimization of the Combustion and Gas Dynamics in High Velocity Suspension Flame Spraying (HVSFS), *Surf. Coat. Technol.*, 2009, **203**(15), p 2139–2145.
75. M. Cuglietta, J. Kuhn and O. Kesler, A Novel Hybrid Axial-Radial Atmospheric Plasma Spraying Technique for the Fabrication of Solid Oxide Fuel Cell Anodes Containing Cu Co, Ni, and Samaria-Doped Ceria, *J. Therm. Spray Technol.*, 2013, **22**(5), p 609–621.
76. G. Bolelli et al., Tribology of NiCrAlY+Al₂O₃ Composite Coatings by Plasma Spraying with Hybrid Feeding of Dry Powder+Suspension, *Wear*, 2015, **344–345**, p 69–85.
77. G. Bolelli et al., “Hybrid” Plasma Spraying of NiCrAlY+Al₂O₃+h-BN Composite Coatings for Sliding Wear Applications, *Wear*, 2017, **378–379**, p 68–81.
78. S. Goel et al., Axial Suspension Plasma Spraying of Al₂O₃ Coatings for Superior Tribological Properties, *Surf. Coat. Technol.*, 2017, **315**, p 80–87.
79. R. Etchart-Salas et al., Influence of Plasma Instabilities in Ceramic Suspension Plasma Spraying, *J. Therm. Spray Technol.*, 2007, **16**(5), p 857–865.
80. Hrabovsky, *Water-stabilized plasma generators*. Pure and Applied Chemistry, 1998, **70**(6): p. 1157-1162.
81. M. Hrabovsky, Thermal Plasma Generators with Water Stabilized Arc, *The Open Plasma Physics Journal*, 2009, **2**, p 99–104.
82. R. Mušálek et al., Feasibility of Suspension Spraying of Ytria-Stabilized Zirconia with Water-Stabilized Plasma Torch, *Surf. Coat. Technol.*, 2015, **268**, p 58–62.
83. R. Musalek et al., Suspensions Plasma Spraying of Ceramics with Hybrid Water-Stabilized Plasma Technology, *J. Therm. Spray Technol.*, 2017, **26**(1), p 37–46.
84. M. Hrabovsky et al., Properties of Hybrid Water/Gas DC Arc Plasma Torch, *IEEE Trans. Plasma Sci.*, 2006, **34**(4), p 1566–1575.
85. M. Shahien and M. Suzuki, Low Power Consumption Suspension Plasma Spray System for Ceramic Coating Deposition, *Surf. Coat. Technol.*, 2017, **318**, p 11–17.

86. H. Hou et al., Vertical Grain and Columnar Structured Ba(Mg/3Ta₂/3)O₃ Thermal Barrier Coating Deposited by Solution Precursor Plasma Spray, *Surf. Coat. Technol.*, 2020, **393**, p 125803.
87. A. Killinger, M. Kuhn and R. Gadow, High-Velocity Suspension Flame Spraying (HVSFS), a New Approach for Spraying Nanoparticles with Hypersonic Speed, *Surf. Coat. Technol.*, 2006, **201**(5), p 1922–1929.
88. H. Kreye, High Velocity Oxy-Fuel Flame Spraying-State of Art, New Developments and Alternatives, *Tagungsunterlagen Conference Proceedings, Erding*, 2003, **2003**, p 5.
89. M. Jadidi, S. Moghtadernejad, and A. Dolatabadi, A Comprehensive Review on Fluid Dynamics and Transport of Suspension/Liquid Droplets and Particles in High-Velocity Oxygen-Fuel (HVOF) Thermal Spray, *Coatings*, 2015, **5**(4), p 576–645.
90. G. Bolelli et al., Properties of Al₂O₃ coatings by High Velocity Suspension Flame Spraying (HVSFS): Effects of injection systems and torch design, *Surf. Coat. Technol.*, 2015, **270**, p 175–189.
91. H. Tabbara and S. Gu, Computational Simulation of Liquid-Fuelled HVOF Thermal Spraying, *Surf. Coat. Technol.*, 2009, **204**(5), p 676–684.
92. M. Oksa et al., Optimization and Characterization of High Velocity Oxy-fuel Sprayed Coatings: Techniques, Materials, and Applications, *Coatings*, 2011, **1**(1), p 17–52.
93. Y. Zhao et al., Influence of Substrate Properties on the Formation of Suspension Plasma Sprayed Coatings, *J. Therm. Spray Technol.*, 2018, **27**(1), p 73–83.
94. B. Bernard et al., Columnar Suspension Plasma Sprayed Coating Microstructural Control for Thermal Barrier Coating Application, *J. Eur. Ceram. Soc.*, 2016, **36**(4), p 1081–1089.
95. F. Caio and C. Moreau, Influence of Substrate Shape and Roughness on Coating Microstructure in Suspension Plasma Spray, *Coatings*, 2019, **9**(11), p 746.
96. P. Sokółowski et al., The Key Process Parameters Influencing Formation of Columnar Microstructure in Suspension Plasma Sprayed Zirconia Coatings, *Surf. Coat. Technol.*, 2014, **260**, p 97–106.
97. P. Sokółowski et al., Advanced Microscopic Study of Suspension Plasma-Sprayed Zirconia Coatings with Different Microstructures, *J. Therm. Spray Technol.*, 2016, **25**(1), p 94–104.
98. P. Fauchais, M. Vardelle and S. Goutier, Latest Researches Advances of Plasma Spraying: From Splat to Coating Formation, *J. Therm. Spray Technol.*, 2016, **25**(8), p 1534–1553.
99. J. Cedelle, M. Vardelle and P. Fauchais, Influence of Stainless Steel Substrate Preheating on Surface Topography and on Millimeter- and Micrometer-Sized Splat Formation, *Surf. Coat. Technol.*, 2006, **201**(3), p 1373–1382.
100. C.-J. Li and J.-L. Li, Transient Contact Pressure During Flattening of Thermal Spray Droplet and its Effect on Splat Formation, *J. Therm. Spray Technol.*, 2004, **13**(2), p 229–238.
101. M.F. Morks et al., Splat Morphology and Microstructure of Plasma Sprayed Cast Iron with Different Preheat Substrate Temperatures, *J. Therm. Spray Technol.*, 2002, **11**(2), p 226–232.
102. K. Yang et al., Study of Substrate Preheating on Flattening Behavior of Thermal-Sprayed Copper Particles, *J. Therm. Spray Technol.*, 2010, **19**(6), p 1195–1205.
103. S.-W. Yao et al., Conditions and Mechanisms for the Bonding of a Molten Ceramic Droplet to a Substrate After High-Speed Impact, *Acta Mater.*, 2016, **119**, p 9–25.
104. F. Tarasi et al., Enhancement of Amorphous Phase Formation in Alumina–YSZ Coatings Deposited by Suspension Plasma Spray Process, *Surf. Coat. Technol.*, 2013, **220**, p 191–198.
105. J. Wang et al., Effect of Substrate Temperature on the Microstructure and Interface Bonding Formation of Plasma Sprayed Ni₂₀Cr Splat, *Surf. Coat. Technol.*, 2019, **371**, p 36–46.
106. K. Pourang, C. Moreau and A. Dolatabadi, Effect of Substrate and Its Shape on in-Flight Particle Characteristics in Suspension Plasma Spraying, *J. Therm. Spray Technol.*, 2016, **25**(1), p 44–54.
107. M. Aghasibeig et al., Fabrication of Nickel Electrode Coatings by Combination of Atmospheric and Suspension Plasma Spray Processes, *Surf. Coat. Technol.*, 2016, **285**, p 68–76.
108. P.G. Lashmi et al., Present Status and Future Prospects of Plasma Sprayed Multilayered Thermal Barrier Coating Systems, *J. Eur. Ceram. Soc.*, 2020, **40**(8), p 2731–2745.
109. S. Mahade et al., Tailored Microstructures of Gadolinium Zirconate/YSZ Multi-Layered Thermal Barrier Coatings Produced by Suspension Plasma Spray: Durability and Erosion Testing, *J. Mater. Process. Technol.*, 2019, **264**, p 283–294.
110. A. Sezavar et al., Thermal Cyclic Fatigue Behavior of Nanostructured YSZ/NiCrAlY Compositionally Graded Thermal Barrier Coatings, *Oxid. Met.*, 2019, **92**(1), p 89–107.
111. A. Sezavar et al., Oxidation Behavior of a Nanostructured Compositionally Graded Layer (CGL) Thermal Barrier Coating (TBC) Deposited on IN-738LC, *Surf. Coat. Technol.*, 2019, **374**, p 374–382.
112. S. Ai et al., Analytical Solution of Quenching-Induced Deposition Stress in Functionally Graded Thermal Barrier Coatings, *Ceram. Int.*, 2019, **45**(9), p 12372–12381.
113. *Reduce processing cost and time using TriplexPro-210 to apply abrasable coatings.* Oelikon Metco (2016)
114. D. Zhou, O. Guillon, and R. Vaßen, Development of YSZ Thermal Barrier Coatings Using Axial Suspension Plasma Spraying, *Coatings*, 2017, **7**(8), p 120.
115. A. Moign et al., Life Cycle Assessment of Using Powder and Liquid Precursors in Plasma Spraying: The Case of Ytria-Stabilized Zirconia, *Surf. Coat. Technol.*, 2010, **205**(2), p 668–673.
116. *Thermal spraying - Determination of the deposition efficiency for thermal spraying.* BS EN ISO 17836 (2017), BSI Standards Limited. p. 8
117. Z. Wang et al., Preparation and Characterization of YSZ Abradable Sealing Coating Through Mixed Solution Precursor Plasma Spraying, *Ceram. Int.*, 2019, **45**(9), p 11802–11811.
118. G. Mittal et al., *Development of Suspension-Based Plasma and HVOF Spray TiO₂ Coatings.* Thermal Spray 2021: Proceedings from the International Thermal Spray Conference, p. 489–492 (2021)
119. Y. Zhao et al., Porous Architecture and Thermal Properties of Thermal Barrier Coatings Deposited by Suspension Plasma Spray, *Surf. Coat. Technol.*, 2020, **386**, p 125462.
120. Y. Yamazaki et al., Improved Thermal Fatigue Resistance in Thermal Barrier Coatings Via Suspension Plasma Spray Technique, *Mater. Lett.*, 2020, **280**, p 128608.
121. A. Ganvir et al., Effect of Suspension Characteristics on the Performance of Thermal Barrier Coatings Deposited by Suspension Plasma Spray, *Ceram. Int.*, 2021, **47**(1), p 272–283.
122. S. Xie et al., Effect of Environmental Pressure on the Microstructure of YSZ Thermal Barrier Coating Via Suspension Plasma Spraying, *J. Eur. Ceram. Soc.*, 2021, **41**(1), p 535–543.
123. A. Ganvir et al., Comparative Study of Suspension Plasma Sprayed and Suspension High Velocity Oxy-Fuel Sprayed YSZ Thermal Barrier Coatings, *Surf. Coat. Technol.*, 2015, **268**, p 70–76.
124. S. Gong et al., Microstructure and Thermal Properties of Inflight Rare-Earth Doped Thermal Barriers Prepared by Suspension Plasma Spray, *J. Eur. Ceram. Soc.*, 2014, **34**(5), p 1243–1253.
125. G. Lyu et al., Fracture Behavior and Thermal Durability of Lanthanum Zirconate-Based Thermal Barrier Coatings with

- Buffer Layer in Thermally Graded Mechanical Fatigue Environments, *Surf. Coat. Technol.*, 2017, **332**, p 64–71.
126. P. Carpio et al., Thermal Behaviour of Multilayer and Functionally-Graded YSZ/Gd₂Zr₂O₇ Coatings, *Ceram. Int.*, 2017, **43**(5), p 4048–4054.
 127. H. Jeon, I. Lee and Y. Oh, Changes in Thermal Conductivity and Thermal Shock Resistance of YSZ-SiO₂ Suspension Plasma Spray Coatings According to Various Raw Material Particle Sizes, *Ceram. Int.*, 2021, **47**(3), p 3671–3679.
 128. W. Ma et al., Microstructure and Thermophysical Properties of SrZrO₃ Thermal Barrier Coating Prepared by Solution Precursor Plasma Spray, *J. Therm. Spray Technol.*, 2018, **27**(7), p 1056–1063.
 129. M. Gell et al., Higher Temperature Thermal Barrier Coatings with the Combined Use of Yttrium Aluminum Garnet and the Solution Precursor Plasma Spray Process, *J. Therm. Spray Technol.*, 2018, **27**(4), p 543–555.
 130. B.-B. Feng et al., Thermophysical Properties of Solution Precursor Plasma-Sprayed La₂Ce₂O₇ Thermal Barrier Coatings, *Rare Met.*, 2019, **38**(7), p 689–694.
 131. R. Kumar et al., Influence of Microstructure on the Durability of Gadolinium Zirconate Thermal Barrier Coatings Using APS & SPPS Processes, *Surf. Coat. Technol.*, 2018, **337**, p 117–125.
 132. X. Ma and P. Ruggiero, Practical Aspects of Suspension Plasma Spray for Thermal Barrier Coatings on Potential Gas Turbine Components, *J. Therm. Spray Technol.*, 2018, **27**(4), p 591–602.
 133. S. Mahade et al., Erosion Performance of Gadolinium Zirconate-Based Thermal Barrier Coatings Processed by Suspension Plasma Spray, *J. Therm. Spray Technol.*, 2017, **26**(1), p 108–115.
 134. R. Kumar et al., Low Thermal Conductivity Yttrium Aluminum Garnet Thermal Barrier Coatings Made by the Solution Precursor Plasma Spray: Part I—Processing and Properties, *J. Therm. Spray Technol.*, 2018, **27**(5), p 781–793.
 135. A. Ganvir et al., Tribological Performance Assessment of Al₂O₃-YSZ composite Coatings Deposited by Hybrid Powder-Suspension Plasma Spraying, *Surf. Coat. Technol.*, 2021, **409**, p 126907.
 136. P. Hameed et al., Axial Suspension Plasma Spraying: An Ultimate Technique to Tailor Ti₆Al₄V Surface with HAP for Orthopaedic Applications, *Coll. Surf. B*, 2019, **173**, p 806–815.
 137. S.T. Aruna et al., A Comparative Study on the Synthesis and Properties of Suspension and Solution Precursor Plasma Sprayed Hydroxyapatite Coatings, *Ceram. Int.*, 2017, **43**(13), p 9715–9722.
 138. S. Mahade et al., Engineered Architectures of Gadolinium Zirconate Based Thermal Barrier Coatings Subjected to Hot Corrosion Test, *Surf. Coat. Technol.*, 2017, **328**, p 361–370.
 139. X. Sun et al., A Study on YSZ Abradable Seal Coatings Prepared by Atmospheric Plasma Spray and Mixed Solution Precursor Plasma Spray, *J. Therm. Spray Technol.*, 2021, **30**(5), p 1199–1212.
 140. J. Marthe et al., Enhancement of Scattering and Reflectance Properties of Plasma-Sprayed Alumina Coatings by Controlling the Porosity, *Surf. Coat. Technol.*, 2013, **220**, p 80–84.
 141. J.-B. Song et al., Improved Reliability of Breakdown Voltage Measurement of Yttrium Oxide Coatings by Plasma Spray, *Ceram. Int.*, 2019, **45**, p 22169–22174.
 142. F.-L. Toma et al., Comparison of the Microstructural Characteristics and Electrical Properties of Thermally Sprayed Al₂O₃ Coatings from Aqueous Suspensions and Feedstock Powders, *J. Therm. Spray Technol.*, 2012, **21**(3), p 480–488.
 143. C. Monterrubio-Badillo et al., Preparation of LaMnO₃ Perovskite Thin Films by Suspension Plasma Spraying for SOFC Cathodes, *Surf. Coat. Technol.*, 2006, **200**(12), p 3743–3756.
 144. D. Soysal et al., Nanostructured Composite Cathodes by Suspension Plasma Spraying for SOFC Applications, *ECS Trans.*, 2019, **35**(1), p 2233–2241.
 145. M. Marr et al., Electrochemical Performance of Solid Oxide Fuel Cells Having Electrolytes Made by Suspension and Solution Precursor Plasma Spraying, *J. Power Sour.*, 2014, **245**, p 398–405.
 146. M. Marr and O. Kesler, Permeability and Microstructure of Suspension Plasma-Sprayed YSZ Electrolytes for SOFCs on Various Substrates, *J. Therm. Spray Technol.*, 2012, **21**(6), p 1334–1346.
 147. M. Marr and O. Kesler, Influence of Plasma Heat Flux on Segmentation Cracking and Permeability of Thin Suspension Plasma Sprayed Coatings, *Surf. Coat. Technol.*, 2013, **216**, p 289–296.
 148. N.S. Waluyo et al., Protective Coating Based on Manganese-Copper Oxide for Solid Oxide Fuel Cell Interconnects: Plasma Spray Coating and Performance Evaluation, *Ceram. Int.*, 2018, **44**(10), p 11576–11581.
 149. S.S. Kumar et al., Solution Precursor Plasma Spray Process: A Promising Route for the Fabrication of Mn-Co Oxide Based Protective Coating for SOFC, *Surf. Coat. Technol.*, 2017, **324**, p 26–35.
 150. J. Wang et al., Oxygen Vacancy Induced Band-Gap Narrowing and Enhanced Visible Light Photocatalytic Activity of ZnO, *ACS Appl. Mater. Interfaces*, 2012, **4**(8), p 4024–4030.
 151. C. Zhang et al., Room-Temperature Nitrogen-Dioxide Sensors Based on ZnO_{1-x} Coatings Deposited by Solution Precursor Plasma Spray, *Sens. Actuators B Chem.*, 2017, **242**, p 102–111.
 152. X. Geng, C. Zhang and M. Debliquy, Cadmium Sulfide Activated Zinc Oxide Coatings Deposited by Liquid Plasma Spray for Room Temperature Nitrogen Dioxide Detection Under Visible Light Illumination, *Ceram. Int.*, 2016, **42**(4), p 4845–4852.
 153. C. Zhang et al., Role of Oxygen Vacancy in Tuning of Optical, Electrical and NO₂ Sensing Properties of ZnO_{1-x} Coatings at Room Temperature, *Sens. Actuators B Chem.*, 2017, **248**, p 886–893.
 154. X. Geng et al., Light Assisted Room-Temperature NO₂ Sensors with Enhanced Performance Based on Black SnO_{1-α}@ZnO_{1-β}@SnO_{2-γ} Nanocomposite Coatings Deposited by Solution Precursor Plasma Spray, *Ceram. Int.*, 2017, **43**(8), p 5990–5998.
 155. R.T. Candidato et al., Effects of Precursor Composition Used in Solution Precursor Plasma Spray on the Properties of ZnO Coatings for CO₂ and UV Light Sensing, *Surf. Coat. Technol.*, 2019, **371**, p 395–400.
 156. A. Abuchenari et al., A Review on Development and Application of Self-Healing Thermal Barrier Composite Coatings, *J. Compos. Comp.*, 2020, **2**(4), p 147–154.
 157. D. Song et al., Crack-Resistance Behavior of an Encapsulated, Healing Agent Embedded Buffer Layer on Self-Healing Thermal Barrier Coatings, *Coatings*, 2019, **9**(6), p 358.
 158. Z. Derelioglu et al., On the Use of B-Alloyed MoSi₂ Particles as Crack Healing Agents in Ytria Stabilized Zirconia Thermal Barrier Coatings, *J. Eur. Ceram. Soc.*, 2015, **35**(16), p 4507–4511.
 159. W. Fan and Y. Bai, Review of Suspension and Solution Precursor Plasma Sprayed Thermal Barrier Coatings, *Ceram. Int.*, 2016, **42**(13), p 14299–14312.
 160. A.L. Carabat et al., Protecting the MoSi₂ Healing Particles for Thermal Barrier Coatings Using a Sol-Gel Produced Al₂O₃ Coating, *J. Eur. Ceram. Soc.*, 2018, **38**(7), p 2728–2734.
 161. N. Sharifi et al., Developing Hydrophobic and Superhydrophobic TiO₂ Coatings by Plasma Spraying, *Surf. Coat. Technol.*, 2016, **289**, p 29–36.

162. Y. Cai et al., Superhydrophobic Ceramic Coatings by Solution Precursor Plasma Spray, *Sci. Rep.*, 2016, **6**(1), p 24670.
163. P. Xu et al., Superhydrophobic Ceramic Coating: Fabrication by Solution Precursor Plasma Spray and Investigation of Wetting Behavior, *J. Colloid Interface Sci.*, 2018, **523**, p 35–44.
164. P. Xu et al., Fabrication of Micro-/Nano-Structured Superhydrophobic Ceramic Coating with Reversible Wettability Via a Novel Solution Precursor Vacuum Plasma Spray Process, *Mater. Des.*, 2018, **160**, p 974–984.
165. P. Xu et al., Efficient One-Step Fabrication of Ceramic Superhydrophobic Coatings by Solution Precursor Plasma Spray, *Mater. Lett.*, 2018, **211**, p 24–27.
166. G. Jnido, G. Ohms and W. Viöl, Deposition of Zinc Oxide Coatings on Wood Surfaces Using the Solution Precursor Plasma Spraying Process, *Coatings*, 2021, **11**(2), p 183.
167. M. Bai et al., Robust Hydrophobic Surfaces from Suspension HVOF Thermal Sprayed Rare-Earth Oxide Ceramics Coatings, *Sci. Rep.*, 2018, **8**(1), p 6973.
168. Z.X. Yu et al., Effect of Precursor Solutions on ZnO Film Via Solution Precursor Plasma Spray and Corresponding Gas Sensing Performances, *Appl. Surf. Sci.*, 2017, **412**, p 683–689.
169. P. Xu et al., Fabrication of Superhydrophobic Ceramic Coatings via Solution Precursor Plasma Spray Under Atmospheric and Low-Pressure Conditions, *J. Therm. Spray Technol.*, 2019, **28**(1), p 242–254.
170. F. Zhang et al., Wettability of Hierarchically-Textured Ceramic Coatings Produced by Suspension HVOF Spraying, *J. Mater. Chem. A*, 2015, **3**(26), p 13864–13873.
171. J. Cizek et al., Silver-Doped Hydroxyapatite Coatings Deposited by Suspension Plasma Spraying, *J. Therm. Spray Technol.*, 2018, **27**(8), p 1333–1343.
172. R.B. Unabia et al., Preliminary Study on Copper-Doped Hydroxyapatite Coatings Obtained Using Solution Precursor Plasma Spray Process, *Surf. Coat. Technol.*, 2018, **353**, p 370–377.
173. M. Chambard et al., Effect of Silver and Strontium Incorporation Route on Hydroxyapatite Coatings Elaborated by rf-SPS, *Materialia*, 2020, **12**, p 100809.
174. R. Sergi et al., Bioactive Zn-Doped Hydroxyapatite Coatings and Their Antibacterial Efficacy Against *Escherichia coli* and *Staphylococcus aureus*, *Surf. Coat. Technol.*, 2018, **352**, p 84–91.
175. L.A. Díaz et al., High-Velocity Suspension Flame Sprayed (HVSFS) Soda-Lime Glass Coating on Titanium Substrate: Its Bactericidal Behaviour, *J. Eur. Ceram. Soc.*, 2016, **36**(10), p 2653–2658.
176. J. Huang et al., Developing Titania-Hydroxyapatite-Reduced Graphene Oxide Nanocomposite Coatings by Liquid Flame Spray Deposition for Photocatalytic Applications, *J. Eur. Ceram. Soc.*, 2017, **37**(12), p 3705–3711.
177. M. Zhai et al., Fabrication of TiO₂-SrCO₃ Composite Coatings by Suspension Plasma Spraying: Microstructure and Enhanced Visible Light Photocatalytic Performances, *J. Therm. Spray Technol.*, 2020, **29**(5), p 1172–1182.
178. Y. Bai et al., Suspension Plasma-Sprayed Fluoridated Hydroxyapatite Coatings: Effects of Spraying Power on Microstructure, Chemical Stability and Antibacterial Activity, *Surf. Coat. Technol.*, 2019, **361**, p 222–230.

Publisher's Note Springer Nature remains neutral with regard to jurisdictional claims in published maps and institutional affiliations.